Structural Engineering Report No. 86

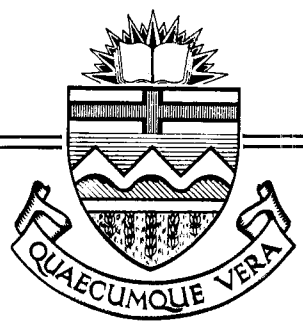

AN INELASTIC ANALYSIS OF THE GENTILLY-2 SECONDARY CONTAINMENT STRUCTURE

by

D. W. MURRAY

C. WONG

S. H. SIMMONDS

J. G. MacGREGOR

April 1980

RECENT STRUCTURAL ENGINEERING REPORTS

Department of Civil Engineering

University of Alberta

57. *A System of Computer Programs for the Large Deformation In-Plane Analysis of Beams* by M. Epstein and D.W. Murray, May 1976.

58. *A Statistical Study of Variables Affecting the Strength of Reinforced Normal Weight Concrete Members* by S.A. Mirza and J.G. MacGregor, December 1976.

59. *The Destabilizing Forces Caused by Gravity Loads Acting on Initially Out-Of-Plumb Members in Structures* by D. Beaulieu and P.F. Adams, February 1977.

60. *The Second-Order Analysis and Design of Reinforced Concrete Frames* by G.S. Mathews and J.G. MacGregor, January 1977.

61. *The Effects of Joint Eccentricity in Open Web Steel Joists* by R.A. Matiisen, S.H. Simmonds and D.W. Murray, June 1977.

62. *Behaviour of Open Web Steel Joists* by R.A. Kaliandasani, S.H. Simmonds and D.W. Murray, July 1977.

63. *A Classical Flexibility Analysis for Gentilly Type Containment Structures* by D.W. Murray, A.M. Rohardt, and S.H. Simmonds, June 1977.

64. *Substructure Analysis of Plane Frames* by A.A. Elwi and D.W. Murray, June 1977.

65. *Strength and Behavior of Cold-Formed HSS Columns* by Reidar Bjorhovde, December 1977.

66. *Some Elementary Mechanics of Explosive and Brittle Failure Modes in Prestressed Containments* by D.W. Murray, June 1978.

67. *Inelastic Analysis of Prestressed Concrete Secondary Containments* by D.W. Murray, L. Chitnuyanondh, C. Wong and K.Y. Rijub-Agha, July 1978.

68. *Strength of Variability of Bonded Prestressed Concrete Beams* by D.K. Kikuchi, S.A. Mirza and J.G. MacGregor, August 1978.

69. *Numerical Analysis of General Shells of Revolution Subjected to Arbitrary Loading* by A.M. Shazly, S.H. Simmonds and D.W. Murray, September 1978.

70. *Concrete Masonry Walls* by M. Hatzinikolas, J. Longworth and J. Warwaruk, September 1978.

71. *Experimental Data for Concrete Masonry Walls* by M. Hatzinikolas, J. Longworth and J. Warwaruk, September 1978.

72. *Fatigue Behaviour of Steel Beams with Welded Details* by G.R. Bardell and G.L. Kulak, September 1978.

73. *Double Angle Beam-Column Connections* by R.M. Lasby and Reidar Bjorhovde, April 1979.

74. *An Effective Uniaxial Tensile Stress-Strain Relationship for Prestressed Concrete* by L. Chitnuyanondh, S. Rizkalla, D.W. Murray and J.G. MacGregor, February 1979.

75. *Interaction Diagrams for Reinforced Masonry* by C. Feeg and J. Warwaruk, April 1979.

76. *Effects of Reinforcement Detailing for Concrete Masonry Columns* by C. Feeg, J. Longworth, and J. Warwaruk, May 1979.

77. *Interaction of Concrete Masonry Bearing Walls and Concrete Floor Slabs* by N. Ferguson, J. Longworth and J. Warwaruk, May 1979.

78. *Analysis of Prestressed Concrete Wall Segments* by B.D.P. Koziak and D.W. Murray, June 1979.

79. *Fatigue Strength of Welded Steel Elements* by M.P. Comeau and G.L. Kulak, October 1979.

80. *Leakage Tests of Wall Segments of Reactor Containments* by S.K. Rizkalla, S.H. Simmonds and J.G. MacGregor, October 1979.

81. *Tests of Wall Segments from Reactor Containments* by S.H. Simmonds, S.H. Rizkalla and J.G. MacGregor, October 1979.

82. *Cracking of Reinforced and Prestressed Concrete Wall Segments* by J.G. MacGregor, S.H. Rizkalla and S.H. Simmonds, October 1979.

83. *Inelastic Behavior of Multistory Steel Frames* by M. EL Zanaty, D.W. Murray and R. Bjorhovde, April 1980.

84. *Finite Element Programs for Frame Analysis* by M. EL Zanaty and D.W. Murray, April 1980.

85. *Test of a Prestressed Concrete Secondary Containment Structure* by J.G. MacGregor, S.H. Simmonds and S.H. Rizkalla, April, 1980.

86. *An Inelastic Analysis of the Gentilly-2 Secondary Containment Structure* by D.W. Murray, C. Wong, S.H. Simmonds and J.G. MacGregor, April 1980.

UNIVERSITY OF ALBERTA

Department of Civil Engineering

AN INELASTIC ANALYSIS OF THE GENTILLY-2 SECONDARY CONTAINMENT STRUCTURE

by

D.W. Murray

C. Wong

S.H. Simmonds

and

J.G. MacGregor

A Technical Report to the

Atomic Energy Control Board

P.O. Box 1046

Ottawa, Canada, K1P 5S9

April 1980

Acknowledgements

The authors wish to acknowledge the cooperation of the following agencies which provided technical information and/or financial support for the overall study.

The Atomic Energy Control Board

Atomic Energy of Canada, Limited

Hydro-Quebec

Canatom Limited

Ontario-Hydro

Disclaimer

The interpretation of the technical data and any opinions or conclusions arising in this report are those of the authors only and do not necessarily reflect those of the co-operating agencies.

Abstract

This report briefly reviews the conceptual development of the analytical technology that has been developed for the overpressure analysis of axisymmetric secondary containment structures at the University of Alberta. It then considers the application of this technology to the analysis of the Gentilly-2 containment structure. The technique of modelling the structure is described in detail and results of the analysis are presented. Conclusions on the performance of the structure, if subjected to overload pressures of arbitrary magnitude, are drawn.

Table of Contents

	Page
Title Page	i
Acknowledgement	ii
Disclaimer	ii
Abstract	iii
Table of Contents	iv
List of Tables	vii
List of Figures	viii
1. Introduction	1
1.1 Background to Report	1
1.2 Review of Project Development	2
1.2.1 Review of Elastic Studies	2
1.2.2 Rationale for Development of Inelastic Technology	3
1.2.3 Review of Development of Inelastic Technology	6
1.2.4 Alternative Technology	8
1.3 Objective of Report	8
2. The Modelling of the Structure	9
2.1 Description of Structure	9
2.2 General Modelling Technique	10
2.3 Modelling the Components	12
2.3.1 Layering	12
2.3.2 Modelling of Foundation and Base Slab (Segments 1 to 11)	13

Page

2.3.3 The Hinge Connection (Segment 12) 14

2.3.4 The Perimeter Wall (Segments 13 and 14) . . 15

2.3.5 The Ring Beam (Segments 15, 16 and 17) . . 16

2.3.6 The Upper Dome (Segments 18, 19 and 20) . . 17

2.3.7 The Lower Dome (Segments 21 and 22) 18

2.4 Material Properties 18

2.5 Load Simulation 22

3. The Structural Analysis 24

3.1 Description of Process 24

3.2 Distribution of Cracking in Structure 25

3.3 Surface Stresses at Proof Load 26

3.4 Stress Resultants 27

3.5 Strain in Reinforcing 28

3.6 Strain in Prestressing Cables 29

3.7 Deflection and Load-Deflection Plots 29

3.8 Estimate of Leakage 29

4. Conclusions and Closure 33

4.1 Conclusions from Analysis 33

4.2 Closure 34

References 36

Tables 38

Figures 44

Appendix A - Equivalent Axisymmetric Prestressing Net 83

A.1 Introduction 83

A.2 Geometry of the Net 83

Page

A.3 Effective Normal Pressure at Crown 84

A.4 Variation in the Normal Pressure 85

A.5 Variation in Stiffness and Strength Properties . . . 86

Appendix B - Ultimate Strength by Membrane Theory 90

List of Tables

Table Number	Title	Page
2.1	Identification of Material Types	38
2.2	Material Types for Segment Layers	39
3.1	Summary of Productive Runs	40
3.2	Leakage Through Dome at Internal Pressure of 72.125 psig	41
3.3	Leakage Through Wall at Internal Pressure of 72.125 psig	42
3.4	Estimated Leakage Rates for G-2 Containment	43
B.1	Component Ultimate Strengths	91

List of Figures

Figure Number	Title	Page
2.1	Reactor Building Section	44
2.2	Reactor Building Prestressing Cable Arrangement	45
2.3	Reactor Building Structural Arrangement	46
2.4	Principal Dimensions of Gentilly-2 Containment	47
2.5	Positive Displacements and Stress Resultants (BOSOR5)	48
2.6	Structural Model: Segment Identification	49
2.7	Connectivity Between Shell Segments	50
2.8	Structural Model: Mesh Point Layout	51
2.9	Reinforcing and Layering for Wall Segments	52
2.10	Reinforcing and Layering for Ring Beam Segments	53
2.11	Reinforcing and Layering for Upper Dome Segments	54
2.12	Reinforcing and Layering for Lower Dome Segments	55
2.13	Stress-Strain for Reinforcing Bars	56
2.14	Stress-Strain for Prestressing Cables	57
2.15	Concrete Stress-Strain: Prestressed Concrete	58
2.16	Tensile Stress-Strain: Reinforced Concrete	59
2.17	Ring Beam and Wall Prestressing Loads	60
2.18	Upper Dome Prestressing Loads	61
2.19	Gravity Loads	62
3.1	Distribution of Cracking at 30 psi	63
3.2	Distribution of Cracking at 50 psi	64
3.3	Distribution of Cracking at 60 psi	65

Figure Number	Title	Page
3.4	Distribution of Cracking at 72.1 psi	66
3.5	Meridional Surface Stresses at Proof Pressure	67
3.6	Circumferential Surface Stresses at Proof Pressure	68
3.7	Variation of N1 Stress Resultant	69
3.8	Variation of N2 Stress Resultant	70
3.9	Variation of M1 Stress Resultant	71
3.10	Meridional Steel Strain: Outer Layer	72
3.11	Meridional Steel Strain: Inner Layer	73
3.12	Circumferential Steel Strain: Outer Layer	74
3.13	Circumferential Steel Strain: Inner Layer	75
3.14	Strain in Meridional Prestressing Cables	76
3.15	Strain in Circumferential Prestressing Cables	77
3.16	Pressure-Displacement at Mid-height of Wall	78
3.17	Pressure-Displacement at Crown of Dome	79
3.18	Normal Displacements	80
3.19	Tangential Displacements	81
3.20	Estimated Leakage Rate	82
A1	Equivalent Prestressing Net	89

1. Introduction

1.1 Background to Report

This report is one of a series of technical reports associated with a program of investigation into the overpressure response of "Gentilly-type" secondary containment structures (hereinafter referred to as G2 containments) sponsored by the Atomic Energy Control Board of Canada. The terminology arises from the fact that the prototype building which served to anchor the study was the containment building for the Gentilly-2 Nuclear Power Station Reactor Building [1]. At the time the study was initiated this building was considered to be representative of secondary containment structures that would be constructed to house 600 MW CANDU-PHW type nuclear power reactors.

The investigation, which continued over a period of approximately five years, consisted of both experimental and analytical studies. These studies were interactive. The objective of the study was to determine as accurately as possible the response to be expected from a containment building of the given type if it were subjected to internal pressure above the proof test pressure, at which it is designed to be free of cracks. A series of limit states, which were measures of deterioration of the structure, were defined [2, pg. 4]. The pressure at which each limit state would be attained was to be determined.

Since the investigation was to study the overall behavior of the structure, many details which could affect localized behavior of the structure were not considered. The structure has been analyzed as axisymmetric with axisymmetric loading. Thus, the effects of the

buttress for anchorage of circumferential prestressing, penetrations, temporary openings, air locks and interior structure have not been considered.

1.2 Review of Project Developments

This report is the last analytical report associated with the project and is concerned with the prediction of the overall behavior to be expected from the G2 containment structure if it were subjected to overpressure. It is considered that the validity of the methodology has been established by previous reports associated with the project. The basis of this argument is contained in the following report of the project.

1.2.1 Review of Elastic Studies

The initial stage of the study dealt with elastic analyses. The effects of gravity loads, prestressing loads, shrinkage, temperature, internal pressure, and construction sequence were included [2]. It was shown that, for the structure under consideration, the effects of creep, shrinkage and construction sequence were small, and although the thermal effect could have significant influence on cracking conditions, it had little influence on ultimate load capcity. The analysis was carried out using the BOSOR4 computer code [3]. It was demonstrated that a very simple computer code based on classical shell theory could be constructed which, except for some specific effects, yields results that are similar to those of BOSOR4 and are adequate for preliminary design and checking purposes [4]. The deficiencies of the classical

analysis are: (a) the effects of tapered thicknesses of shell elements on the distribution of stress resultants cannot be included, and (b) short segments of spherical shells cannot be properly handled. In addition the stiffening effect of the reinforcing steel is difficult to include. Unreported finite element studies confirmed the adequacy of these elastic analyses within the limitations of the elastic assumptions.

While elastic analyses give a good indication of the condition of the structure prior to cracking, their extrapolation to post-cracking conditions cannot provide accurate information on subsequent limit states. Estimates of these limit states were made on the basis of such extrapolations using simple strength design concepts [2]. For these estimates it was necessary to assume that post-cracking stress resultants and/or deformations were proportional to their precracking values. The estimates were carried out with quasi-uniaxial assumptions [2] and with more complex biaxial assumptions [5], but no assurance could be given that the results were reliable. The actual behavior of the structure can only be predicted from a full nonlinear analysis.

1.2.2 Rationale for Development of Inelastic Technology

The remainder of the project was devoted to developing a technology that could give reliable results for post-cracking response of containment structures, from the time of crack initiation until ultimate failure.

Since the maximum pressure that could be developed within the structure was not known to the investigators, and indeed would be dependent upon the nature of the failures that were assumed to occur in

the safety systems, a hypothetical pressure which could develop the full capacity of the structure was assumed. This poses certain difficulties in interpretation of results since the final failure of the structure loaded internally by a compressible medium would be explosive if it were leak-tight at the time it reached its ultimate capacity [6,7].

Obviously, however, an unlined containment structure strained to its maximum load carrying capacity would be extensively cracked and, therefore, would not be leak-tight. The real response of the structure to internal pressurization becomes a rate-dependent problem. The maximum pressure that could be developed internally would be reached if the rate of leakage from the building were to equal the rate of delivery of the pressurizing medium to the building. Although the investigators are not in a position to carry out such an interactive analysis they were in a position to attempt to obtain data which would provide basic input to such a study. One aspect of the investigation was, therefore, to obtain as accurate an estimate as possible of the cracking to be expected in the structure at various load levels. In order to obtain accurate estimates of cracking it is necessary that the analysis properly predict strains. This required that a technology to predict post-cracking strains in prestressed concrete thinshell structures be developed, since no satisfactory technology was available at the initiation of the project.

In view of the preceeding considerations the following strategy was adopted. An analytical technique would be developed to predict average strains in cracked prestressed concrete membrane elements. The

necessary material properties would be deduced from laboratory tests of elements (called "wall segments") similar to those which would exist in a typical containment structure (approximately 1/4 scale). The material model would be refined to the extent that the best correlation possible would be obtained for a variety of these specimen types.

The analytical technique would then be applied to a test structure which would subsequently be constructed and tested to failure in the laboratory. The test structure would be approximately 1/14 the size of a Gentilly-2 containment structure and, although it could not be a scale model of this structure, would have components modelled to simulate similar behavior. A good correlation between the strains predicted by the analytical technique and those measured on the test structure would establish the validity of the technique as a valid tool to assess the behavior of the Gentilly-2 containment.

In addition to assessing the state of stress and strain within the structure for arbitrary internal pressures, an attempt to estimate leakage would be made using the following methodology. Crack widths and spacings would be measured on all wall segment tests and a correlation of this crack geometry with measured strains would be inferred. Leakage through similar specimens would be measured and related to the inferred crack geometry. Based on the strains obtained for the G2 structure using the analysis contained in this report the crack geometry-strain relationship would then be used to estimate cracking of the G2 structure and the leakage relationship applied to obtain an estimate of leakage for this structure.

While it is apparent that there is an intimate interaction between the analytical development described above and the testing phases of the project, it should be pointed out that the testing phases of the project could be regarded as independent of any analytical development. The testing phases of the project included such things as the effect of lapped bar splices which are difficult to model analytically. In addition, the observation of the behavior of the test structure would provide valuable insight about the behavior of a containment structure without any analysis. However, integrating the two phases of the project enhances interpretation of the results from each phase.

1.2.3 Review of Development of Inelastic Technology

The essential elements of the development of the technology described in Sect. 1.2.2 have been completed. An elastic-plastic material model for concrete which determines average strains through the assumption of tensile stiffening and permits independent softening in two orthogonal directions was developed in Reference 8. When this material description was incorporated into the BOSOR5 computer code [9] it provided an analytical technique which enabled strains to be closely simulated for the biaxial stress conditions in two of the wall segment specimens [8,10].

Subsequent attempts to refine those initial estimates of material properties [11] produced little change in the initially recommended softening curve. This analysis of data indicated that the shape of the softening curve produced little effect on the predicted

behavior. However, the assumed tensile strength of the concrete had a very significant effect on behavior. In general it was found that the effective tensile strength that could be developed in the prestressed segment was only approximately 60% of that measured by standard test procedures [11,12]. Detailed documentation of all segment tests is reported in Reference 21. Comparison of nonprestressed segments with prestressed segments indicated that the effective tensile strength associated with the former type of construction is substantially lower than that which can be developed for the prestressed construction.

The analytical technique developed for the analysis of the segments was considered to be satisfactory and, therefore, the technique was applied to the analysis of the test structure. The development of the technique of modelling the structure is described in Reference 8. After all material properties of the test structure were determined this modelling technique was then applied in a final analysis of the test structure which yielded concrete strains which the investigators consider to be in excellent agreement with the test results [13,14]. A comprehensive comparison of predicted and measured behavior of the test structure is contained in Reference 15.

Two "wall segments" were loaded in tension and the rate of leakage of air through the cracked section was measured [16]. While some difficulties were encountered in maintaining a pressure in one of the tests, from the successful test an empirical constant was determined which can be used to estimate the rate of flow of air through an "equivalent crack width" which can be determined from average strains. Which this relationship the rate of leakage of air from an overpressured containment can be estimated.

1.2.4 Alternative Methodology

An alternative technology for determining the overpressure response of axisymmetric containments was developed in parallel with the technology described in Sect. 1.2.3. This work was unsponsored but has been applied to the analysis of the wall segment tests and the test structure with equally good results.

This work consisted of the development of a hypoelastic concrete constitutive relationship, which emphasized the softening relationship in tension but which is quite generally applicable to three dimensional inelastic concrete response [17]. This constitutive relationship was incorporated into a specially written axisymmetric isoparametric finite element program. The program uses linear, quadratic or cubic serendipity elements and steel layers in the meridional and circumferential directions can be independently specified within each element. Prestressing effects can be specified in a natural way in association with any steel layer. The results obtained from an analysis of the test structure by this technology are compared in Reference 18 with those obtained in Reference 8.

1.3 Objective of Report

The objective of this report is to apply the technology developed through this project, as summarized in Sect. 1.2.3, to the analysis of the Gentilly-2 secondary containment structure, and to draw conclusions therefrom about the behavior of the structure if it were to be subjected to internal pressure up to its ultimate capacity.

2. The Modelling of the Structure

2.1 Description of the Structure

The Gentilly-2 secondary containment structure is a prestressed concrete structure, composed of "thin" shell elements, and having an overall height of 168 ft. and outside diameter of 143 ft. A vertical section through the structure is given in Fig. 2.1. The principal components of the containment consist of:

(a) a circular base slab 5 ft. thick and approximately 155 ft. in diameter,

(b) a vertical cylinder of 68 ft. inside radius with a wall thickness of 3.5 ft., and

(c) a spherical dome cap of 2 ft. thickness, an inner radius of 136 ft., and an angle at the springing line of approximately 30°.

Other significant aspects of the structure which must be considered in the modelling are:

(a) an inner spherical dome is located approximately 9 ft. below the outer spherical dome. This dome has a center opening with a fence or parapet around it and serves as the bottom of a reservoir for the storage of dousing water.

(b) the thickness of the cylinder wall is approximately doubled between the two domes to create a ring beam.

(c) both domes are tapered into the cylinder wall.

(d) the internal structure is separated from the containment components of the structure.

(e) four vertical buttresses, of thickness equal to that of the ring beam, are located 90° apart on the cylinder wall to serve as anchorages for the circumferential prestressing cables.

(f) the cylinder wall is joined to the base with a Freyssinet hinge.

(g) the base slab is underlain by a concrete sub-base separated from the base slab by a membrane which permits radial movements.

A schematic of the prestressing system is shown in Fig. 2.2, and some basic features of the building are shown in Fig. 2.3.

2.2 General Modelling Technique

Since the computer program developed for the analysis of the test structure was a modified version of BOSOR5, the model must be compatible with the capabilities of this program. Hence the structure is modelled as axisymmetric, which means that the effect of the buttresses is neglected. This technique is justified on the basis that it produced good results for overall behavior of the test structure in all areas except in the immediate vicinity of the buttresses. The effects of the buttresses on overall behavior was small and is discussed further in Reference 15.

The principal geometry upon which the computer model for the G-2 structure is based is shown in Fig. 2.4 while the BOSOR5 sign convention for displacements and stress resultants is shown in Fig. 2.5.

The structure is modelled as a series of shell segments which are defined with respect to a reference surface. In accordance with the

experience of modelling the test structure [8,14] a continuous reference surface was used for the containment components of the structure. An overall view of the model, with the component segments identified, is shown in Fig. 2.6. Some geometric details, including the linkage between components, are shown in Fig. 2.7.

The segments are layered to represent the different materials as one passes through the thickness of a component. The general technique of modelling the reinforcement and prestressing cables is the same as described in References 8 and 14. Each layer of reinforcing or prestressing steel is modelled as a separate layer with thickness equal to that necessary to provide the same area per unit width as provided by the bars on cables. Bar cut-offs are tapered over a development length in accordance with the experience acquired in the test structure analysis.

Mesh points are assigned to any location on the reference surface which defines a section at which output of displacements, stresses and strains is desired. Mesh points must also be assigned to any point where it is necessary to specify a change of thickness of the section or a layer or a change in loading conditions. The number of intermediate mesh points between the above control points is selected by the analyst such that, in his judgement, the model will be able to adequately represent the variation of stresses and strains. The mesh points are generally more closely spaced near the ends of structural components where the restraints imposed by adjacent components may induce bending in addition to the membrane forces. The distribution of

mesh points for the model of Fig. 2.6 is shown in Fig. 2.8, and the number of points associated with each component is summarized in the table in Fig. 2.6.

Loadings are simulated by distributed pressures applied to the reference surface, either normal or tangential to the surface, or by concentrated loads acting at the mesh points. The prestressing loads were simulated as distributed pressures, except for anchorage forces and circumferential cable forces in the ring beam, which were simulated as concentrated forces. Consequently, it was necessary to reduce the yield stress in the prestressing layers to an effective value as described in reference 8.

The following sections describe the modelling in more detail.

2.3 Modelling the Components

2.3.1 Layering

Layering of components is controlled by the arrangement of the steel in the structure. This requires that the locations and areas of layers of reinforcing and prestressing steel be read from the construction drawings and transformed into equivalent layers in the model. While this appears to be a simple but tedious task, there is a considerable amount of judgement involved because of the limited arrangement of layering permitted by the BOSOR5 code. The region of greatest complexity is the ring beam area which is shown in Fig. 2.10 and will be discussed in more detail in Sect. 2.3.5. Since all minor variations of reinforcement cannot possibly be included, the reinforcement and

prestressing which have been interpreted by the authors to be representative of that for the components have been assigned to the components. A summary of the number of layers and the material associated with each of these layers in each component is given in Tables 2.1 and 2.2. The specification of the thickness and location of each layer at each station in each component was considered to be too voluminous to be reproduced in this report, and hence has been omitted.

2.3.2 Modelling of Foundation and Base Slab (Segments 1 to 11)

The modelling of the rock subgrade for a BOSOR5 analysis is probably the least well-defined aspect of the modelling procedure. The technique employed for the BOSOR4 analyses of Ref. 2 was questioned on the basis that it yielded moments that were too large at the base of the cylinder wall. The modelling technique employed for the current model is an improved version of the technique applied in Ref. 2.

Since the stresses in the base are not of interest in themselves, any technique to model the foundation can be used provided it yields the proper interactive effect in the sense of translational and rotational restraint at the base of the wall. Consequently the foundation is modelled as an axisymmetric Winkler foundation in which the restraint to the base slab is concentrated at a discrete number of points. The 'spring elements' supporting these discrete points are BOSOR5 cylindrical shell elements hinged at the bottom and the top. Eleven such elements were used as shown in Fig. 2.6. The thickness of each of the supporting elements is such that they are contiguous on a radial line. More of these support shells are used in the vicinity of

the wall location than towards the centerline of the structure. The axial stiffness, and outer radius, associated with these supporting components was adjusted by trial until the vertical displacement, rotation and moment at the base of the cylinder wall, under gravity load, corresponded to those obtained from an elastic finite element analysis in which the base was included in the model.

The base slab was modelled as a circular plate of 5 ft. thickness and 77'-9" outside radius. The thickness of the slab was reduced to 4'-10" at the connection with the wall, and increased to 5'-3" for radii exceeding 72'-6", in an attempt to model the geometry of the real structure as closely as possible. The reference surface for the base slab is located 2 in. below the top slab, as shown in Figs. 2.6 and 2.7, to eliminate the need for a rigid link connection at the junction between the base and the wall.

The base slab is assumed elastic throughout the analysis with stiffness properties equal to those of uncracked concrete.

2.3.3 The Hinge Connection (Segment 12)

The connection of the wall to the top of the base slab was modelled as a short cylindrical segment of 3 inch length with constant thickness of 18 inches. Five layers of steel were used to model the reinforcing and prestressing through this component, which, when combined with the intermediate concrete layers, yields a total of 11 layers as shown in Fig. 2.9C. Since the dowels, which are #9 at 12" as shown in Fig. 2.9B, are inclined, only the vertical component of the steel force has been assumed to yield effective reinforcing in the meridional

direction. The vertical prestressing steel has been determined based on 124 vertical cables of 77 wires each distributed uniformly around the circumference at the junction.

Two layers of circumferential steel have been added to yield the same effective steel ratio in the circumferential direction as in the wall immediately above the hinge. No circumferential prestressing steel is considered.

Based on experience gained from analyses of the test structure [8], and preliminary analyses of the current structure, an elastic-perfectly plastic concrete relationship in both tension and compression is used in the hinge component in place of the degrading (softening) curves used for the concrete in the remainder of the structure. The precaution is required because the large curvatures arising in the hinge area at high loads may produce numerical instabilities in the solution, if softening response is included in this area. Convergence problems result from this effect.

2.3.4 The Perimeter Wall (Segments 13 and 14)

Two segments, numbers 13 and 14, have been used to model the perimeter wall. Both segments are 3'-6" thick, but because of additional reinforcement in the bottom 9'-6" of the wall, extra layers are required in this region. For segment 13, fifteen layers (the maximum that can be used) have been employed to simulate the design. The meridional layers combine the dowels from the base (#9 @ 12"), the nominal vertical reinforcing (#9 @ 12") and the V shaped reinforcing across the bottom of the wall (assumed to be #6 @ 12"). This is a combination of the

reinforcing indicated in Figs. 2.9A and B. The circumferential reinforcing has been assigned on the basis of #11 @ 12" for the inside of the wall, with #11 @ 6" for the bottom 3 feet and #10 @ 12" for the remaining 6'-6" on the outside of the wall. The vertical prestressing is that specified for segment 12 while the horizontal prestressing assumes that 69 cables of 85 wires are uniformly distributed over a height of 138'-9".

Segment 14 has been modelled in 11 layers. Since the reinforcing varies along the length, the thickness of the layers varies accordingly. The reinforcing used is shown in Fig. 2.9. Prestressing is the same as for segment 13.

2.3.5 The Ring Beam (Segments 15, 16 and 17)

The ring beam is approximately 7 ft. wide and 14 ft. high. The inner face tapers into both the lower and the upper dome. It serves to anchor the vertical wall prestressing and the dome prestressing. It is the most difficult part of the containment to model.

The mesh layout, assumed reinforcing, and layering of this area are shown in Fig. 2.10. In an attempt to simulate the connections to the three adjoining segments, to accommodate the three different prestressing systems passing through it, and to simulate the complex reinforcing, the beam has been divided into three segments, each with 15 layers. A continuous reference surface has been maintained and a tapered transition section at the connection with the wall has been introduced, based on the experience of modelling the test structure [8,14].

Segment 15 is a cylindrical shell of variable thickness, 8.585 ft. long. Sixteen mesh points, with average spacing of approximately 0.6 ft., have been used. The variable thickness is specified in such a way as to avoid overlapping with the lower dome which is connected to this segment by a rigid link as shown in Figs. 2.7 and 2.10. The reinforcing steel has been condensed into 4 meridional layers and two circumferential layers. Steel associated with anchorage of dome prestressing cables has not been included.

Segments 16 and 17 are variable thickness components with reference surface on a circular arc. They serve to join segment 15 to the upper dome. Two segments must be used because the intersection of the prestressing layers cannot occur within a segment (a limitation imposed by the BOSOR5 code). The radius of the reference surface is 4.903 ft. Each has 9 mesh points. The steel has again been condensed in each segment so that only 15 layers are required. These layers are indicated in Fig. 2.10. Judgement has been used in assigning the steel to equivalent layers. The details of layering are too involved to present in this report. However, the layering is based upon the steel indicated in Fig. 2.10. The segments and layers are of variable thickness and eccentric from the reference surface, as may be seen in Fig. 2.10.

2.3.6 The Upper Dome (Segments 18, 19 and 20)

The upper dome attaches to the ring beam at the springing line at an angle of approximately 30°. It is prestressed by a net of 3 layers of cables running on great circles approximately 60° apart. This prestressing net has been converted into equivalent circumferential and

meridional steel by using the methodology of Sect. 3.3.2 of Ref. 8. The calculations for the conversion are given in Appendix A.

The dome has been modelled in three segments as shown in Figs. 2.6 and 2.11. The middle surface has a radius of 137 ft. and the prestressing net has been located on this surface. Each segment has ten layers. The steel associated with each layer of reinforcing is given in the table in Fig. 2.11. The meridional reinforcement reduces in steps as one travels along a meridian towards the crown. Segment 18 has been tapered, eccentrically from the reference surface, to represent the smooth transition from the dome to the ring beam.

2.3.7 The Lower Dome (Segments 21 and 22)

The lower dome is the only unprestressed component above the foundation. It has been modelled by two segments as shown in Figs. 2.6 and 2.12. The dome has a uniform thickness of 1'-3" except in the immediate vicinity of the springing line. A short cylinder with a length of 4.15 ft. has been used to model the fence. Eight layers have been used for each component with the steel being assigned to be equivalent to the reinforcing shown in the table in Fig. 2.12. The meridional steel is again reduced stepwise as one travels along the meridian towards the crown.

2.4 Material Properties

The three materials which have been incorporated into the model are reinforcing steel (ASTM A615-Grade 60), prestressing steel (ASTM A421-65 Type BA), and 5000 psi concrete.

The reinforcing steel is assumed to follow an elastic-perfectly plastic stress-strain relationship with a modulus of elasticity of 29.6×10^6 psi and a yield stress of 60 ksi. These properties are illustrated in Fig. 2.13. They are associated with material types 2 and 3 and have been assigned to the component layers as indicated in Table 2.2.

The prestressing steel properties are indicated on the stress-strain curve in Fig. 2.14 which is simulated by five linear sections. The minimum ultimate strength (f_{pu}) is assumed as 255 ksi. The elastic limit is assumed to be 70% of f_{pu} with an effective modulus of elasticity (E) of 29.0×10^6 psi. The offset strain of 0.2% is assumed to be reached at 80% of f_{pu}. Above 90% of f_{pu} the tangent modulus was reduced to 0.1 E, a value that was not reduced further because a positive stiffness of the concrete-steel cross-section must be maintained to avoid numerical instabilities. For large strains the only elements of the structure which contribute positively to the stiffness are the prestressing cables.

Since the method of simulating prestressing effects is to apply external pressure and line loads (see Sect. 2.5), only the reserve capcity of the prestressing steel can be developed when subjected to live load strains. To account for this the origins of the stress-strain curves are shifted to the initial stress levels (f_{pi}) as illustrated in Fig. 2.14 [8]. Since these initial stress levels vary with the structural component it is necessary to input three different stress-strain curves for the prestressing. Considering the directional stiffness properties

of the prestressing layers, this gives rise to the four material types, designated as types 4, 6, 7 and 8 in Table 2.1, and associated with the layering of components as indicated in Table 2.2.

The concrete is considered to have a cylinder strength of 5000 psi (f'_c = 5000 psi) and a tensile strength (f'_t) of $6\sqrt{f'_c}$ [11]. The modulus of elasticity is assumed to be $57000\sqrt{f'_c}$ [19], and the Poisson's ratio to be 0.2 [8]. Three different concrete material types are included in the model. For each concrete material two stress-strain curves, one for compression and one for tension, are specified.

The concrete types used in the model are as follows.

(a) Prestressed Concrete

This material is assumed for all concrete other than the hinge and the lower dome (i.e. segments 12, 21 and 22) and is designated as Material 5 in Figures and Tables. The tensile curve shown in Fig. 2.15A, is a piecewise linear curve which follows that recommended in Ref. 11 for 5000 psi concrete. This curve, includes the following control values.

(i) $f'_t = 6\sqrt{f'_c}$ (424 psi)

(ii) $f''_t = 0.6\ f'_t$ at $\varepsilon = 0.00012$ (254 psi)

(iii) $\sigma = 0.45\ f''_t$ at the elastic limit (114.5 psi)

(iv) $\sigma = 0.90\ f''_t$ at $\varepsilon = 0.0003$ (229 psi)

The compression curve also is piecewise linear and follows the recommendations of Ref. 11. This curve is shown in Fig. 2.15B and includes the following control values.

(i) $f''_c = 0.85\ f'_c$ at $\varepsilon_o = 2f''_c/E$

(ii) $\sigma = 0.45\ f''_c$ at the elastic limit

(iii) $\sigma = 0.85\ f''_c$ at $\varepsilon = 0.0038$

(iv) Control points between $0.45\ f''_c$ and f''_c fall on the curve $\sigma = f''_c \{\frac{2\varepsilon}{\varepsilon_o} - (\frac{\varepsilon}{\varepsilon_o})^2\}$

(b) Hinge Concrete

The concrete in the hinge (segment 12) designated in Figures and Tables as Material 1 is assumed to be elastic-perfectly-plastic to avoid possible numerical instabilities arising from the response at this location (see Sect. 2.3.3). The yield value in compression is assumed to be f''_c as indicated in Fig. 2.15B. The yield value in tension is assumed to be 42 psi which is the residual tensile stress attributed to the prestressed concrete at a strain of 0.0038. This value is indicated in Fig. 2.15A.

(c) Reinforced Concrete

The concrete in the lower dome, which is the bottom of the dousing reservoir, is unprestressed. The evidence from the experimental phase of this project indicates that the tensile stress which can be developed in reinforced concrete is substantially lower than that which can be developed in prestressed concrete. Ref. 11 suggests that a value of $0.3f'_t$ may be appropriate. Consequently, it is assumed for the lower dome that $f''_t = 0.3\ f'_t$. When the recommendations of Ref. 11 are applied to a concrete with this peak tensile strength (127 psi) the tensile curve of Fig. 2.16 results. The compressive curve that has been used is identical to that for prestressed concrete, as indicated in Fig. 2.15B. This concrete is material 9 of Tables 2.1 and 2.2.

2.5 Load Simulation

BOSOR5 permits the application of distributed pressure, and concentrated loads and moments, to the reference surface. A time history curve then controls the magnitude of the basic loading condition. In the original program, both the distributed normal pressure and tangential pressure for a segment were controlled by the same time-history curve. The investigators modified this to allow independent variation of tangential and normal pressures. However, the fact that only one normal pressure and one tangential pressure can be specified for a segment still restricts the versatility of loading and controls the method of inputting gravity loads for the dome.

The system of loads is illustrated in Figs. 2.17, 2.18 and 2.19. Internal (live load) pressure, which is specified as a normal pressure in the reference surface of all segments of the (outer) containment components of the structure, is not illustrated in these figures.

The prestressing loads are indicated in Figs. 2.17 and 2.18. A uniform normal pressure of 5.29 k/ft^2 is applied to the cylinder reference surface as indicated in Fig. 2.17. The normal pressure on the dome is uniform for each dome segment but varies from segment to segment, as shown in Fig. 2.18, to account for the gradual variation in normal pressure resulting from the distortion of the geometry of the prestressing net as one travels along the meridian (see Appendix A). The prestressing cables are assumed to be straight once they enter the ring beam segments. Their anchorage close to the outer edge of the beam results in an inclined line load as shown in Fig. 2.18. This force is

then replaced by a set of statically equivalent forces and moments acting at three mesh points on the reference surface as indicated in the table of Fig. 2.17. This technique was determined to be effective in the analysis of the test structure [8,14].

In a similar manner, the anchorage of the vertical perimeter wall cables is simulated by a set of statically equivalent forces and moments acting at three mesh points on the reference surface as indicated in the table of Fig. 2.17. The equilibrating force at the bottom of the perimeter wall, which has been applied at node 12-1, is also included in the table.

The prestressing forces from the eight circumferential tendons in the ring beam, shown in Fig. 2.10, account for the remainder of the forces in the table of Fig. 2.17. When the reference surface forces from these four sources are combined, loads and/or moments are applied at the nodes indicated in Fig. 2.17.

The dead load of the lower dome is applied as a combination of normal and tangential distributed forces varying according to the formula of Fig. 2.19. The dead load of the fence and the perimeter wall are applied as tangential distributed forces as indicated in Fig. 2.19. However, since the dead loads of the upper dome and the upper segments of the ring beam have both tangential and normal components, and since the normal pressure on the reference surface will be a variable because it is the means of applying the internal pressure, it is not possible with the BOSOR5 input to specify the dead loads of these segments as pressure loads. Therefore statically equivalent concentrated loads, as indicated in Fig. 2.19, have been used to simulate the weight of these dome and ring beam segments.

3. The Structural Analysis

3.1 Description of Procedure

The procedure for analysis of the Gentilly-2 containment structure is the same as that developed for the test structure and which has been summarized in Ref. 8. Load increments are applied one at a time with each load increment requiring an individual run. The state of the structure at the end of the load increment is written into a file which is retained and this information provides the input for the next run. This "restart capacity" permits iteration to be continued at the same load level, or to be restarted from any of the previous converged positions with a smaller load increment if convergence difficulties are encountered. Generally there is significant interaction between the analyst and the solution process as the analysis proceeds, and considerable engineering judgement is required to successfully carry it out in such a way so as to minimize the number of nonproductive runs. The output is voluminous and good file manipulation techniques are required. Any small errors in input generally are not in evidence until the structure has undergone significant inelastic behavior. At this time small perturbations in geometry or material characteristics, or details of the modelling procedure, may begin to dominate the solution. Such effects, arising from the details of modelling, have been discussed in References 8 and 14.

A summary of the productive runs for this analysis is contained in Table 3.1. The analysis was discontinued at a pressure of 72.125 because of convergence difficulties. An upper bound on the ultimate load is shown in Appendix B to be 77.2 psi.

Thus, although the analysis was terminated at 93% of this value the nature of the structural behaviour at failure is evident.

3.2 Distribution of Cracking in the Structure

The progressive states of cracking in the structure are shown in Figs. 3.1 to 3.4 for internal pressures of 30, 50, 60 and 72.125 psi, respectively. As anticipated, 'horizontal' cracking occurs first on the inside face and is located at the springing line of the dome. First cracking is actually indicated on the section through mesh point 18-2 of the upper dome at a pressure of 27.5 psi. However, at 30 psi this cracking has little penetration as can be seen from Fig. 3.1. Since the inner dome is not a part of the containment from a point of view of leakage, this type of cracking has little significance and it is, therefore, questionable whether this concept of 'first cracking' has any relevance to a containment design. It is, however, a convenient computation which gives a very conservative index to ensure against more significant cracking.

Fig. 3.2 indicates the distribution of cracking at 50 psi. internal pressure. Approximately one half of the dome has through-cracks in both the vertical and circumferential directions at this pressure. No through-cracking exists in the wall of the structure.

At 60 psi (Fig. 3.3) all but the bottom of the cylinder wall has throughcracks. The region of vertical cracking in the dome appears to have stabilized but horizontal cracking has spread throughout practically all of the dome structure. Fig. 3.4 shows that at 72 psi vertical through-cracks exist throughout the cylinder wall while other cracking regions are also somewhat extended.

Some concern has been expressed about the possibility of the lower dome "breaking loose" from the ring beam at higher internal pressures and falling as a rigid body. From Fig. 3.4 it is seen that there are no vertical cracks in either the ring beam or lower dome at an internal pressure of 72.125 psig and that the circumferential or horizontal cracks in the lower dome do not penetrate through the section. In addition an examination of Fig. 3.18 indicates that the normal displacements (outward movement) of the ring beam at the junction with the lower dome is very small even at very high pressures. For these reasons and the construction details there is little probability that the lower dome can break loose from the ring beam.

3.3 Surface Stresses at Proof Load

The distribution of surface stress at the proof test pressure is shown, for both the inside and outside surfaces, on Figs. 3.5 and 3.6. Fig. 3.5 shows stresses in the meridional direction. Tension is indicated on the inside of the structure at the springing line of the dome and on the outside of the structure at the junction of the wall with the ring beam. However, both of these tensile stresses are below the cracking stress (254 psi). Hence, the analysis indicates that the structure satisfies the specific requirement that no cracking should occur under proof load. (Cracking of the lower dome does not affect leakage from the containment.)

Tensile stresses may be somewhat higher in regions near the ring beam as a result of creep within the cross-section, a condition

which has not been considered in this analysis. However in view of the subsequent crack pattern under further pressurization (Fig. 3.2) it is apparent that throughcracks first appear in the upper section of the dome. At proof loads the stresses in this region of the dome have substantial compressive values in both directions (Figs. 3.5 and 3.6), and therefore are not influenced by the localized tensile stresses appearing in Fig. 3.5.

3.4 Stress Resultants

The stress resultants, N1, N2 and M1 (see Fig. 2.5) are shown in Figs. 3.7 to 3.9, respectively, for five different load levels.

In general the stress resultants are not of fundamental interest in this type of analysis, other than giving some inforation relative to statics checks. All stress resultants are produced by the program by integrating the stresses across the cross-section.

Throughout most of the wall and dome the inplane stress resultants are reasonably uniform and the bending moments, except in the region near the ring, are small, conforming to anticipated shell behavior.

Fig. 3.7 indicates that there is a perturbation of the N1 force within the region of sharp curvature of the reference surface in the transition from the ring beam to the dome. The details of this area are shown in Fig. 2.10. There are rapid changes in thickness and discontinuities in the layering. The results within this region may, therefore, be somewhat suspect. Fortunately this area does not appear to be a critical area. A similar perturbation is even more pronounced

in the N2 force shown in Fig. 3.8 and is again attributed to discontinuities in modelling rather than to behavior of the structure.

The severe perturbation in the M1 stress resultant near the dome to ring beam joint is caused by the shift of the reference surface relative to the center of resistance of the cross-section and does not reflect the moment about the centroid of the section.

3.5 Strain in Reinforcing

The strain in the outer and inner reinforcing layers in both the meridional and circumferential directions is shown in Figs. 3.10 to 3.13 for five different load levels. The material properties of Fig. 2.14 must be used in conjunction with these strain diagrams to obtain the associated stresses. The peak strain in the inner layer of reinforcing steel at the pressure of 72.1 psi is spurious and can be disregarded. It is caused by an input error in which the steel layer deviated by less than 0.001 ft. from its required alignment. It can be seen that this effect does not have an influence on the strains in the other three layers of steel (Figs. 3.10, 3.12 and 3.13).

For convenience the yield strain in tension is plotted on each figure. It is apparent from these diagrams that at 72.1 psi yielding of the meridional steel occurs only over very limited regions of the structure whereas the circumferential steel is strained well beyond yield over the majority of the structure.

3.6 Strain in Prestressing Cables

The strain in the prestressing cables is shown in Figs. 3.14 and 3.15 for five different loading conditions. The strain spike in the

meridional prestressing in the dome at 72.1 psi (Fig. 3.14), is again spurious, for the reasons stated in Sect. 3.5, and should be disregarded. The vertical lines labelled 70%, 75% and 80% are the strains corresponding to these percentages of f_{pu} or points 2, 3, and 4, respectively on the stress-strain diagram given in Fig. 2.14. As discussed in the test structure study [8,14], it is evident that a structure which cracks in the manner indicated in Fig. 3.4 is behaving primarily as a tension structure. In this case the prestressing cables form a net which controls the ultimate strength of the structure. It is evident from Figs. 3.14 and 3.15 that final failure of the structure is a simple circumferential extension of the cylinder wall. This failure pressure is computed in Appendix B.

3.7 Deflections and Load-Deflection Plots

Figure 3.16 contains a plot of the lateral displacement at mid-height of the cylinder wall as the pressure increases. Fig. 3.17 shows a similar plot for vertical displacement at the top of the dome. Both displacements are approximately 0.5 ft at 72.1 psi.

Figures 3.18 and 3.19 show the plots of normal displacement and tangential displacement, respectively, against the meridional coordinate measured with respect to the bottom of the wall, for five different normal pressures.

It is considered sufficiently accurate to interpolate displacements at intermediate pressures, since this will yield conservative estimates.

3.8 Estimate of Leakage

The determination of the rate of leakage from the containment once through-the-wall cracking exists is not part of the structural

analysis. However the analysis provides gross strains at each section which, using a methodology developed in other parts of the overall study, permits an estimation of crack widths and thus leakage rates. Since the relationships postulated in this methodology are based on limited data, only an order-of-magnitude estimate of leakage will be attempted.

3.8.1 Calculation of Length and Width of Cracks

The calculations of crack widths are based on procedures presented in Chapter 6 of Ref. 20. The following assumptions were made in calculating the spacing and width of cracks:

(a) The fully developed crack pattern would include two through-cracks converging on every tendon in the wall or the dome.

(b) A fully developed crack pattern exists in every region where the average surface strain on the most highly strained surface exceeds 0.002.

(c) The first cracks develop at every fifth final crack location at a tensile strain of 0.00012.

(d) As the strains increase from 0.00012 to 0.002 additional cracks develop.

(e) The crack width governing leakage is a function of the smaller surface strain at the crack location.

(f) In the dome the potential crack locations are divided into "circumferential cracks", following the tendons in hexagonal lines concentric about the top of the dome and "meridional cracks" following all other tendon lines. The widths of these two groups are governed by the meridional and circumferential strains, respectively.

The width of "equivalent cracks" are then obtained from the expression

$$w = \varepsilon \cdot s$$

where s is the crack spacing obtained as above

ε is the smaller of the surface strains perpendicular to the crack as obtained from the BOSOR5 analysis.

The total length of each through crack of a given width were obtained for internal pressures of 50, 60, 64, 67, 70 and 72.125 psig. Typical of these calculations are the results for 72.125 psig which are given in Table 3.2 and 3.3. From these values the rate of leakage can be estimated.

3.8.2 Calculation of Leakage

A procedure for estimating the leakage of air for a given pressure differential through an equivalent crack of known width is given in Reference 16. The estimate of leakage contained herein is based on air as the gas which is leaking through the cracked containment wall and the evaluation of an equivalent crack width as outlined in the previous section. It is also assumed that the internal pressure during the evaluation of leakage is constant. No attempt has been made to carry out studies of the interaction between volume of containment, rate of build-up of internal pressure, crack widths and leakage.

The rate of leakage is obtained using the expression derived in Reference 16.

$$Q = \frac{p}{C} \sum_{i=1}^{j} w_i^3$$

where w_i is the width of equivalent crack

p is the pressure gradient

C is a constant dependent on the thickness of wall, length of crack, and viscosity of the fluid.

3.8.3 Magnitude of Leakage

The rate of leakage from the G2 containment was estimated at internal pressures of 50, 60, 64, 67, 70 and 72.125 psig and are tabulated in Table 3.4. It is seen that prior to an internal pressure of 50 psig or more than twice the design basic accident pressure there is no appreciable leakage of the containment. As the reinforcement begins to yield the cracks are permitted to open and the rate of leakage increases exponentially. This is seen in Fig. 3.20 in which the rate of leakage is plotted logarithmically.

At the pressure at which the analysis was terminated a volume of air equal to the volume of the containment could leak in approximately one second. At the estimated pressures at failure approximately four times the volume of the containment would leak in one second. These values are based on leakage through cracks in the concrete only and do not consider leakage through the hinge at the base of the wall or through penetrations in the containment. Thus it would appear that pressures approaching say 68 psig may be obtained inside the containment but that at higher pressures the rate of leakage would be such that failure by fracture of the tendons (77 psig) is unlikely.

4. Conclusions and Closure

4.1 Conclusions from Analysis

The following conclusions relative to the overpressure response of a Gentilly-2 type containment may be drawn from this analysis.

1. Excluding possible localized failures, due to details of the penetrations, the ultimate strength of a G2 containment is approximately 77 psi. It, therefore, has a load factor against ultimate failure of approximately 4.3 with respect to basis of design basis accident conditions, or 3.7 with respect to the proof pressure. (See Appendix B).
2. Excluding possible localized failures, the mechanism of failure is simple extension of the cylinder wall, as a result of membrane circumferential tension. That is, moments and discontinuities play no role in the ultimate failure of the structure, and it acts as a simple tension structure. The failure load can, therefore, be computed "on the back of an envelope." (See Appendix B).
3. Although there is tension in the concrete under the proof pressure, these tensions are below the cracking strength of the concrete. In any case they are not associated with a mode that extends to through-cracking and, therefore, are of no consequence.
4. First through-cracking occurs in the dome at a pressure of 48 psi. This pressure is the best estimate of that at which significant leakage would commence.
5. Significant yielding of the reinforcing steel occurs in the circumferential direction in the cylinder wall at a pressure of 66 psi.

This represents the pressure beyond which the structure may be incapable of "resealing itself."

6. A positive compressive membrane force exists at the springing line of the lower dome throughout the total history of pressurization. The lower dome is effected very little by pressurization and shows no distress.

7. The analysis has no capability of predicting spalling of concrete from the surface, or loosening of concrete from the reinforcing mesh. However, spalling is usually associated with compressive failures and there are no significant compressive stress areas developed on the inside of the structure. Furthermore, spalling did not occur during any of the experimental phases of the project. It is the judgement of the investigators that spalling is not a problem.

8. Normal and tangential displacements of the reference surface are shown in Figs. 3.18 and 3.19 for a number of internal pressures. These can serve as a basis for estimating displacements at any intermediate pressure, by interpolation between the curves.

9. No appreciable leakage will occur for internal pressures below 50 psig. However at pressures above say 70 psig the rate of leakage is such that it is unlikely that greater internal pressures will be realized.

4.2 Closure

The investigators consider that the primary objectives of this project have been met. That is, that a technology has been developed

which allows the inelastic behavior of a secondary containment structure to be determined in detail up to its ultimate load.

This technology indicates that, as far as the overall response is concerned, the G2 structure would behave in a perfectly satisfactory manner if subjected to internal pressure overloads. This assumes that proper precautions are taken to eliminate possible premature local failures.

REFERENCES

1. "Safety Report: Gentilly-2 600 mw Nuclear Power Station", Report to the Atomic Energy Control Board for Hydro-electrique de Québec, Atomic Energy of Canada Limited.

2. Epstein, M. and Murray, D.W., "An Elastic Stress Analysis of a Gentilly Type Containment Structure: Volume 1", Structural Engineering Report No. 55, Department of Civil Engineering, University of Alberta, Edmonton, Canada, April 1976.

3. Bushnell, D., "Stress, Stability and Vibration of Complex Branched Shells of Revolution: User's Manual for BOSOR4", Lockheed Missile and Space Company, Inc., Sunnyvale, California.

4. Rohardt, A.M., Murray, D.W., and Simmonds, S.H., "A Classical Flexibility Analysis for Gentilly Type Containment Structures", Structural Engineering Report No. 63, Department of Civil Engineering, University of Alberta, Edmonton, Canada, June 1977.

5. Koziak, B.D.P., and Murray, D.W., "Analysis of Prestressed Concrete Wall Segments", Structural Engineering Report No. 78, Department of Civil Engineering, University of Alberta, Edmonton, Canada, June 1979.

6. Murray, D.W., "Some Elementary Mechanics of Explosive and Brittle Failure Modes in Prestressed Containments", Structural Engineering Report No. 66, Department of Civil Engineering, University of Alberta, Edmonton, Canada, June 1978.

7. Murray, D.W., "A Review of Explosive Characteristics of Prestressed Secondary Containments Near the Ultimate Load", Nuclear Engineering and Design, Vol. 52, Amsterdam, 1979.

8. Murray, D.W., Chitnuyanondh, L., Wong, C., and Rijub-Agha, K.Y., "Inelastic Analysis of Prestressed Concrete Secondary Containments", Structural Engineering Report No. 67, Department of Civil Engineering, University of Alberta, Edmonton, Canada, July 1978.

9. Bushnell, D., "BOSOR5 - A Computer Program for Buckling of Elastic-Plastic Complex Shells of Revolution Including Large Deflections and Creep; Vol. 1: User's Manual, Input Data", Lockheed Missiles and Space Company, Inc., Sunnyvale, California, December, 1974.

10. Murray, D.W., Chitnuyanondh, L., Rijub-Agha, K. and Wong C., "Concrete Plasticity Theory for Biaxial Stress Analysis", Journal of the Engineering Mechanics Division, American Society of Civil Engineers, New York, December 1979.

11. Chitnuyanondh, L., Rizkalla, S., Murray, D.W. and MacGregor, J.G., "An Effective Uniaxial Tensile Stress-Strain Relationship for Prestressed Concrete", Structural Engineering Report No. 74, Department of Civil Engineering, University of Alberta, Edmonton, Canada, February 1979.

12. Chitnuyanondh, L., Rizkalla, S., Murray, D.W. and MacGregor J.G., "Effective Tensile Stiffening in Prestressed Concrete Wall Segments", Paper J3/4, SMIRT5, Berlin, August 1979.

13. Simmonds, S.H., MacGregor, J.G., and Murray, D.W., "Progress Report - Test of the Laboratory Containment Structure", Department of Civil Engineering, University of Alberta, Edmonton, Canada, January 1979.

14. Rizkalla, S., Simmonds. S.H., and MacGregor, J.G., "A Test of a Model of a Thin-Walled Prestressed Concrete Secondary Containment Structure", Paper J4/2, SMIRT5, Berlin, August 1979.

15. MacGregor, J.G., Simmonds, S.H., and Rizkalla, S.H., "Test of a Prestressed Concrete Secondary Containment Structure", Structural Engineering Report No. 85, Department of Civil Engineering, University of Alberta, Edmonton, Canada, March 1980.

16. Rizkalla, S.H., Simmonds, S.H. and MacGregor, J.G., "Leakage Tests of Wall Segments of Reactor Containments", Structural Engineering Report No. 80, Department of Civil Engineering, University of Alberta, Edmonton, Canada, October 1979.

17. Elwi, A.A. and Murray, D.W., "A 3D Hypoelastic Concrete Constitutve Relationship", Journal of the Engineering Mechanics Division, American Society of Civil Engineers, New York, August 1979.

18. Elwi, A.A., "Nonlinear Analysis of Axisymmetric Reinforced Concrete Structures", Ph.D. Thesis, Department of Civil Engineering, University of Alberta, Edmonton, Alberta, Spring 1980.

19. "Building Code Requirements for Reinforced Concrete, ACI 318-77", American Concrete Institute, Detroit, 1977.

20. MacGregor, J.G., Rizkalla, S.H., and Simmonds, S.H., "Cracking of Reinforced and Prestressed Concrete Wall Segments", Structural Engineering Report No. 82, Department of Civil Engineering, University of Alberta, Edmonton, Canada, March 1980.

21. Simmonds, S.H., Rizkalla, S.H., and MacGregor, J.G., "Tests of Wall Segments from Reactor Containments", Structural Engineering Report No. 81, Department of Civil Engineering, University of Alberta, Edmonton, Canada, November 1979.

Table 2.1

Identification of Material Types

Material Number	Description
1	Concrete: Elastic-Plastic: f''_t = 42 psi f''_c = 4250 psi
2	Mild Steel (circumferential): f_y = 60 ksi
3	Mild Steel (meridional): f_y = 60 ksi
4	Wall Vertical Strand: $f_{pi} = 0.601\ f_{pu}$
5	Concrete: Degrading: f'_t = 424 psi f'_c = 5000 psi
6	Wall and Ring Beam Circumferential Strand: $f_{pi} = 0.573\ f_{pu}$
7	Dome Meridional Strand: $f_{pi} = 0.55\ f_{pu}$
8	Dome Circumferential Strand: $f_{pi} = 0.55\ f_{pu}$
9	Concrete for Unprestressed Segments: $f''_t = 0.3\ f'_t$

Table 2.2

Material Types in Each Layer of Segment

Segment \ Layer	1	2	3	4	5	6	7	8	9	10	11	12	13	14	15
12	1	2	1	3	1	4	1	3	1	2	1				
13	5	2	3	5	3	5	4	5	3	5	6	5	3	2	1
14	5	2	3	5	4	5	6	5	3	2	5				
15	5	3	2	5	3	5	4	5	3	5	6	5	2	3	1
16	5	3	2	5	4	5	3	5	7	5	6	5	2	3	1
17	5	3	2	5	7	5	3	5	4	5	6	5	2	3	1
18	5	3	2	5	7	8	5	2	3	5					
19	5	3	2	5	7	8	5	2	3	5					
20	5	3	2	5	7	8	5	2	3	5					
21	9	2	3	9	9	3	2	9							
22	9	2	3	9	9	3	2	9							

Note - For identification of Material Type number see Fig. 2.1.

Table 3.1

Summary of Productive Runs

Step	Load (psig)	Load Increment	No. of Trials
1	Half of Gravity Load	-	2
2	Gravity Load	-	3
3	Gravity and Prestress		4
4	6.0	6.0	3
5	12.0	6.0	3
6	18.0	6.0	3
7	20.7	2.7	3
8	27.5	6.8	3
9	30.0	2.5	4
10	32.5	2.5	3
11	35.0	2.5	3
12	37.5	2.5	3
13	40.0	2.5	3
14	43.0	3.0	4
15	46.0	3.0	5
16	48.0	2.0	4
17	50.0	2.0	5
18	52.5	2.5	7
19	55.0	2.5	7
20	57.5	2.5	6
21	60.0	2.5	5
22	62.0	2.0	5
23	64.0	2.0	4
24	66.0	2.0	5
25	67.0	1.0	6
26	68.5	1.5	8
27	70.0	1.5	10
28	71.0	1.0	7
29	71.5	0.5	4
30	71.75	0.25	2
31	72.00	0.25	8
32	72.125	0.125	6

Table 3.2 Leakage Through Dome at Internal Pressure of 72.125 psig

Length of Crack feet	Width of Equivalent Crack inches	Leakage cu.ft./sec.
1611	0.002002	2648
2369	0.001737	2542
1254	0.002000	2053
394	0.018150	281801
1659	0.001760	1852
942	0.002107	1806
408	0.001759	455

Table 3.3 Leakage Through Wall at Internal Pressure of 72.125 psig

Length of Crack feet	Width of Equivalent Crack inches	Leakage cu.ft./sec.
25	0.000199	0
40	0.000390	0
40	0.000629	1
64	0.000915	6
176	0.001319	47
700	0.002933	2065
756	0.003869	5122
864	0.004806	11219
864	0.005781	19534
864	0.006716	30626
864	0.007582	44065
864	0.008367	59217
864	0.009064	75282
864	0.009670	91384
864	0.010179	106599
864	0.010629	121377
1728	0.011032	271389
1728	0.011256	288297
1728	0.011178	282383
1728	0.010818	255935
864	0.010326	111306
864	0.009823	95806
864	0.009274	80614
864	0.008632	65023
864	0.007903	49886
864	0.007091	36044
864	0.006213	24242
864	0.005292	14985
864	0.004354	8343
864	0.003421	4046
704	0.002517	1313
480	0.001706	279
180	0.001090	27
96	0.000696	4
40	0.000475	1
17	0.000369	0
10	0.000320	0

Table 3.4 Estimated Leakage Rates for G-2 Containment

Internal Pressure	Rates of Leakage cu.ft./sec.		
psig	Dome	Wall	Total
50	4	-	4
60	537	3,463	4,000
64	1,760	27,440	29,200
67	3,530	123,170	126,700
70	6,600	826,900	833,500
72.125	493,200	2,156,400	2,649,600

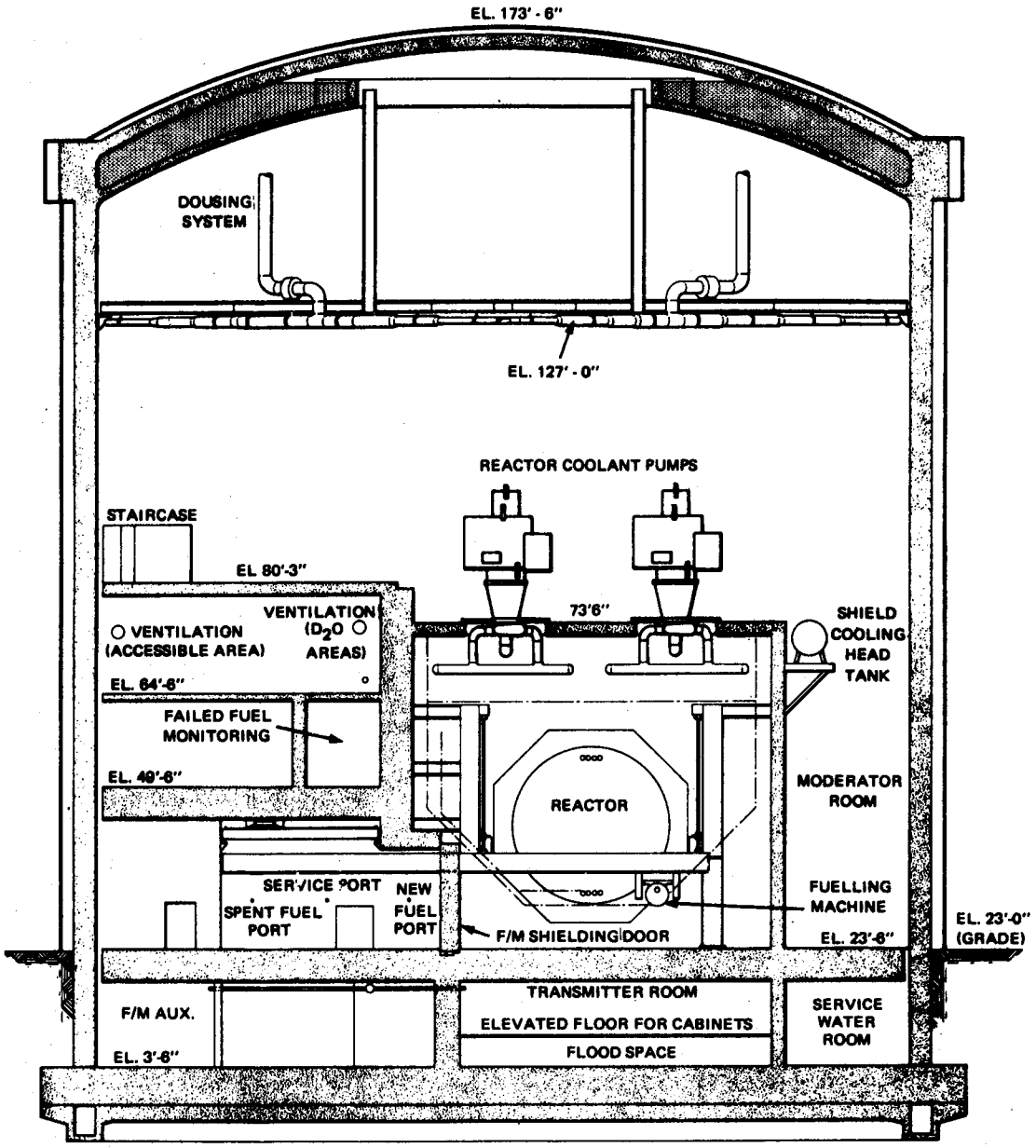

Fig. 2.1 Reactor Building Section

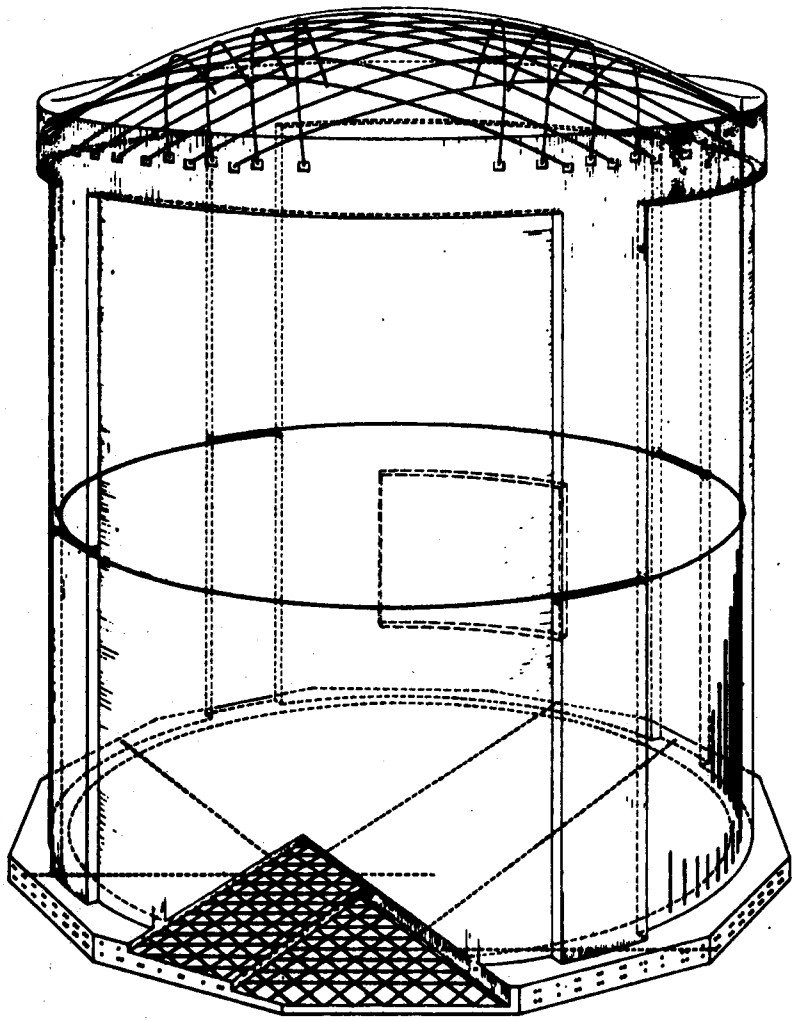

Fig. 2.2 Reactor Building Prestressing Cable Arrangement

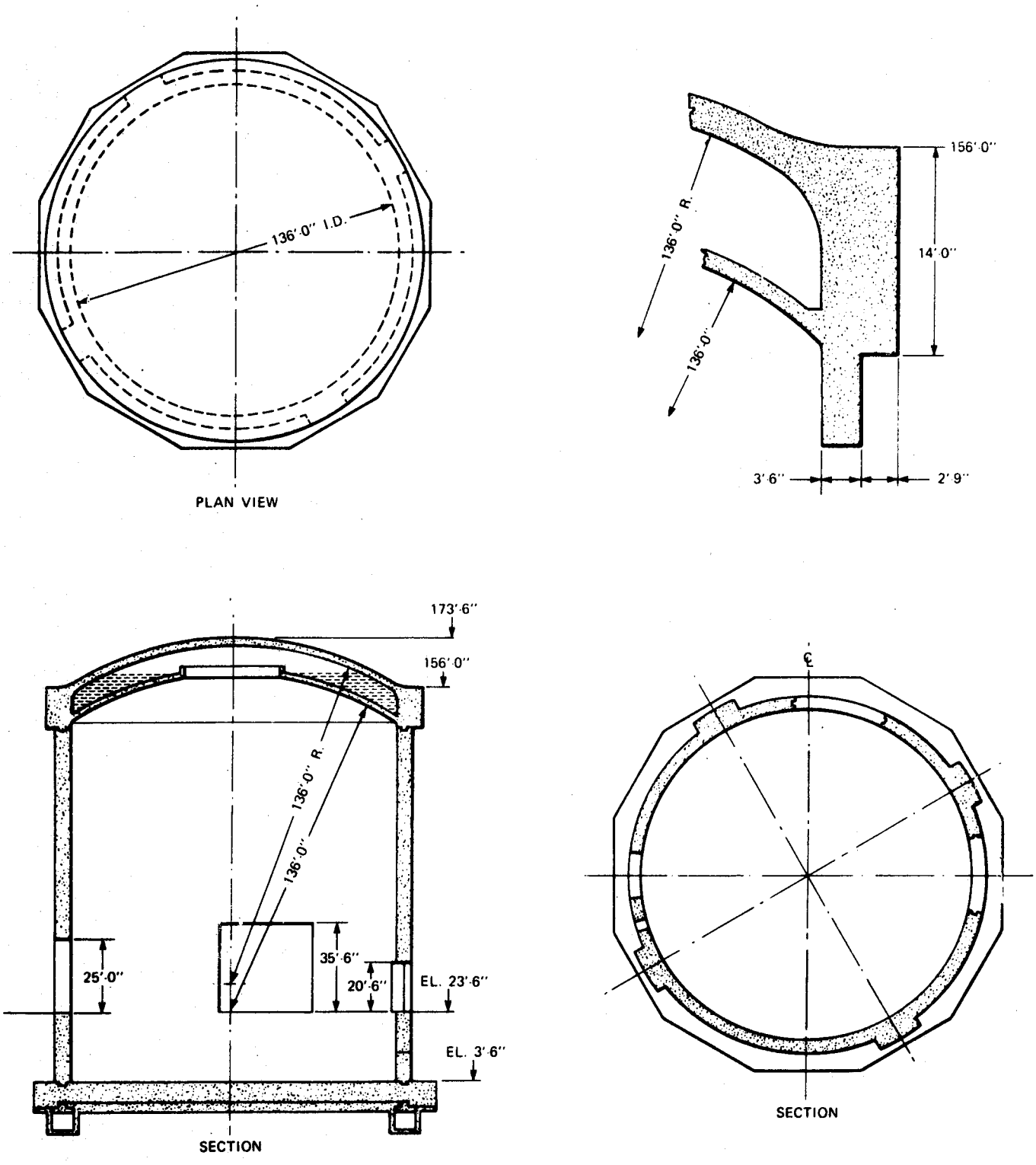

Fig. 2.3 Reactor Building Structural Arrangement

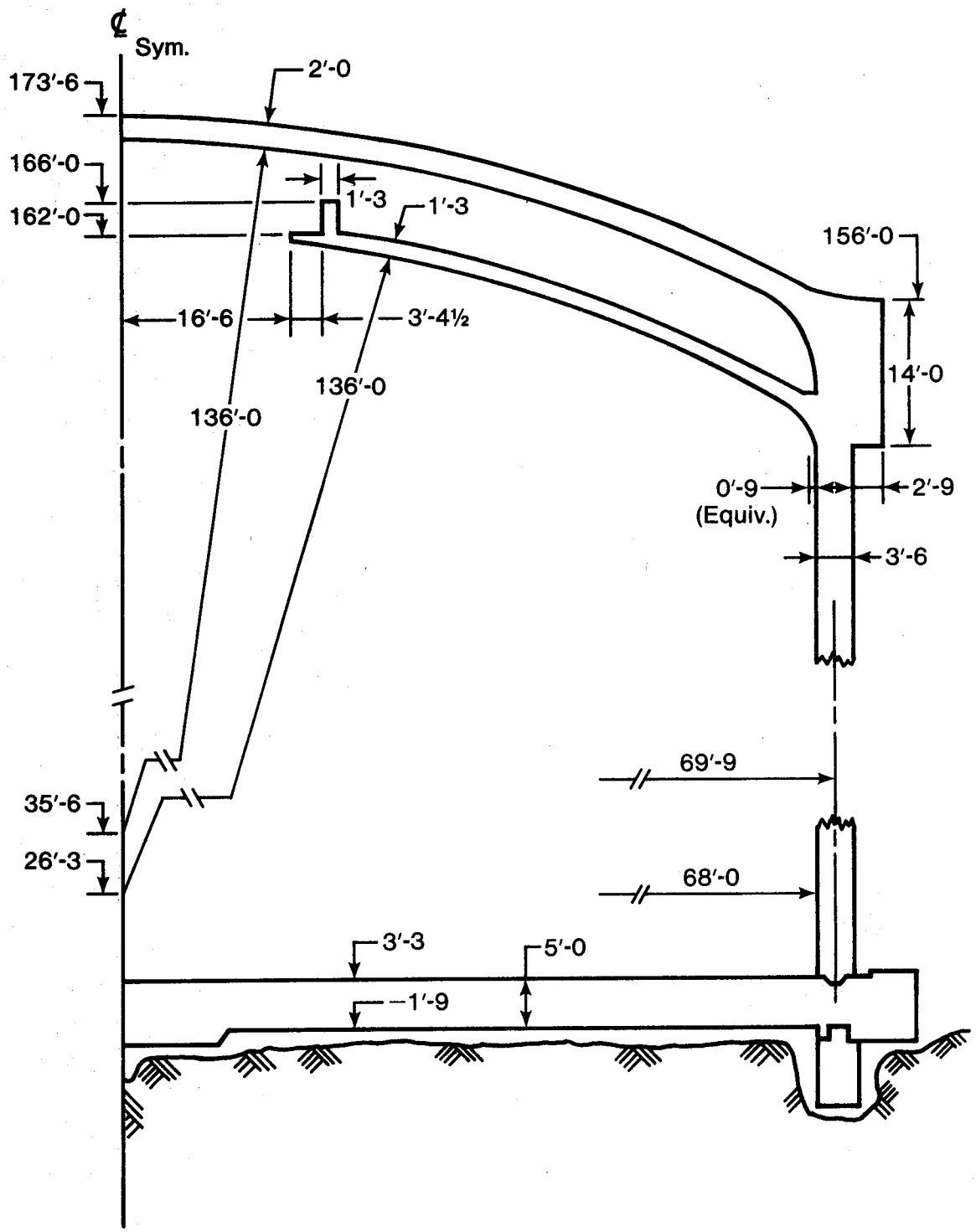

Fig. 2.4 Principal Dimensions of Gentilly-2 Containment

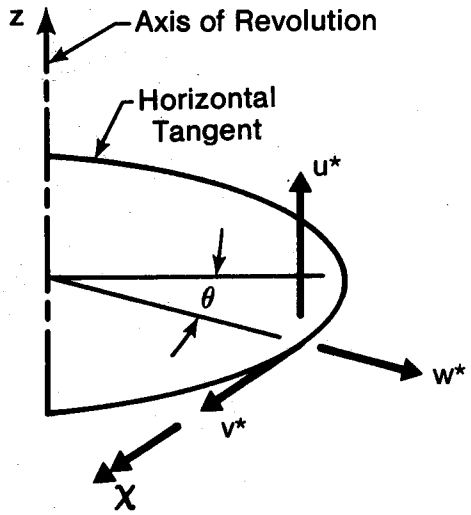

(a) Global Displacements

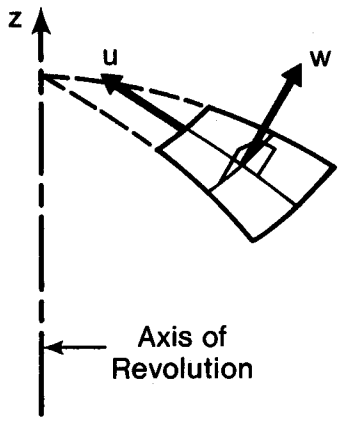

(b) Local Displacements

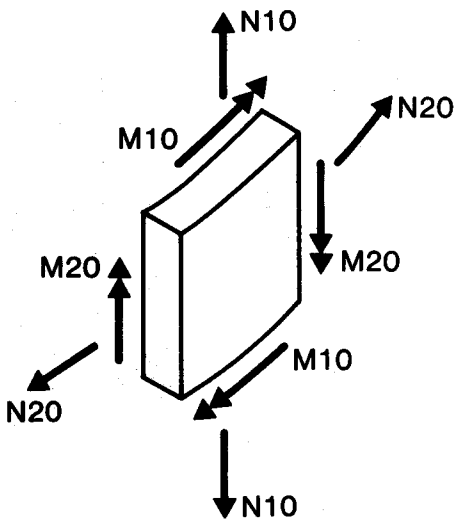

(c) Cylinder Stress Resultants

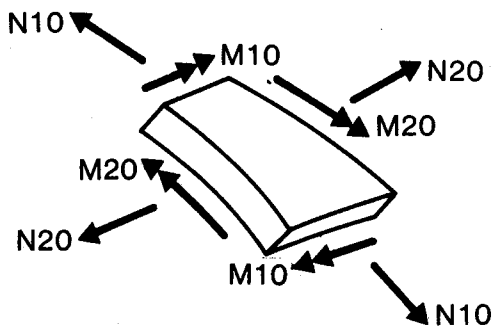

(d) Dome Stress Resultants

Fig. 2.5 Positive Displacements and Stress Resultants (BOSOR5)

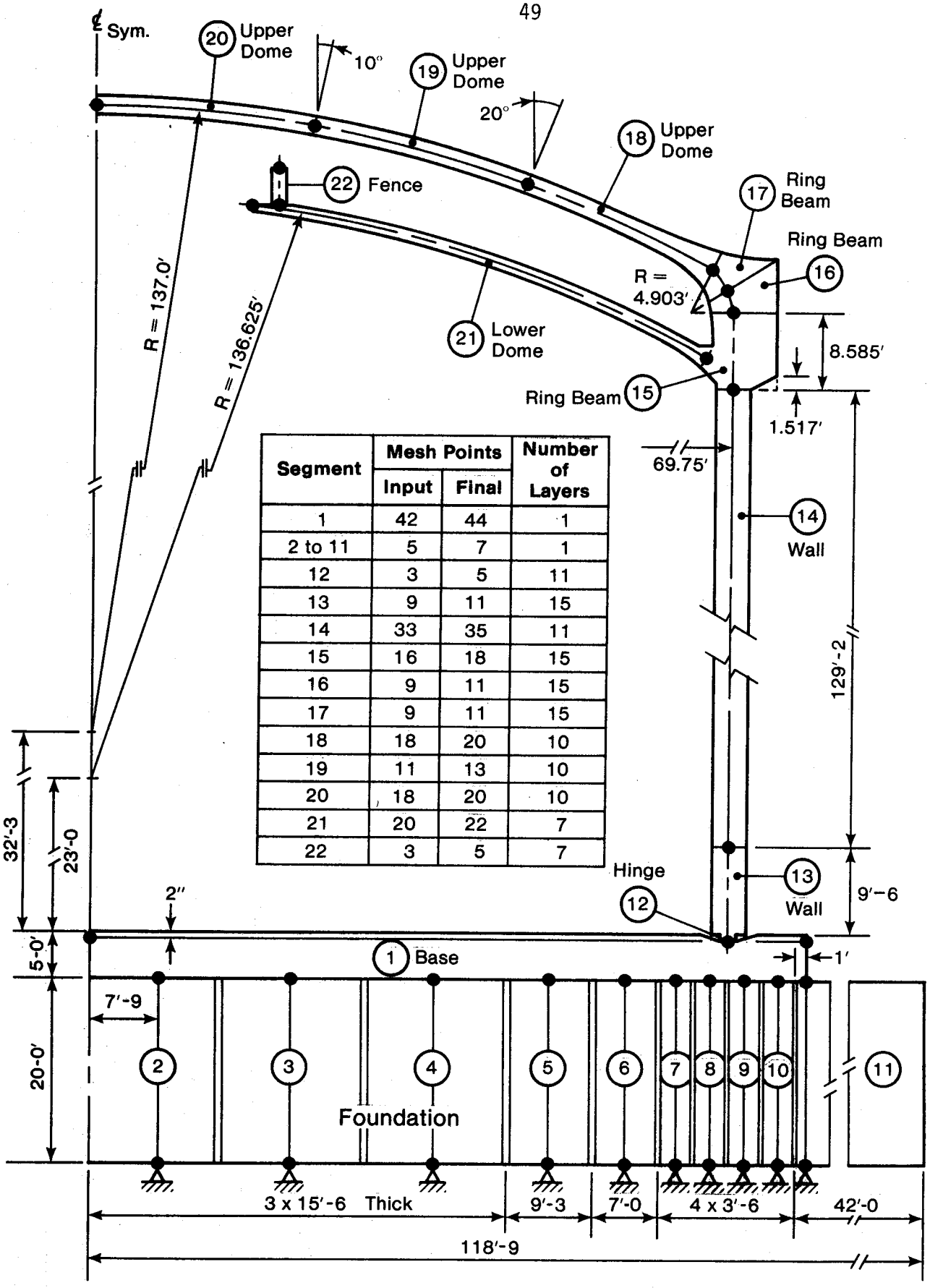

Segment	Mesh Points		Number of Layers
	Input	Final	
1	42	44	1
2 to 11	5	7	1
12	3	5	11
13	9	11	15
14	33	35	11
15	16	18	15
16	9	11	15
17	9	11	15
18	18	20	10
19	11	13	10
20	18	20	10
21	20	22	7
22	3	5	7

Fig. 2.6 Structural Model: Segment Identification

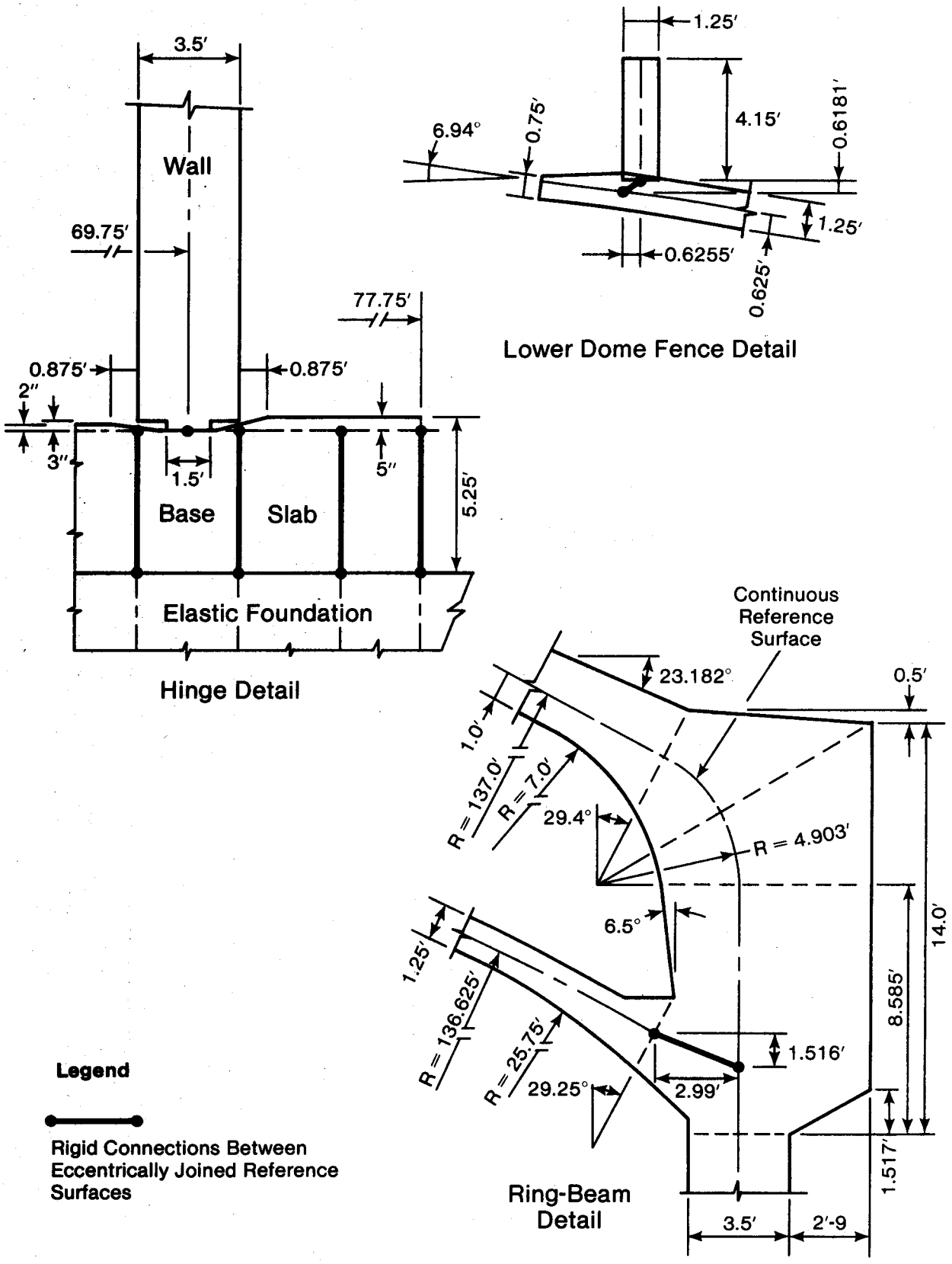

Fig. 2.7 Connectivity Between Shell Segments

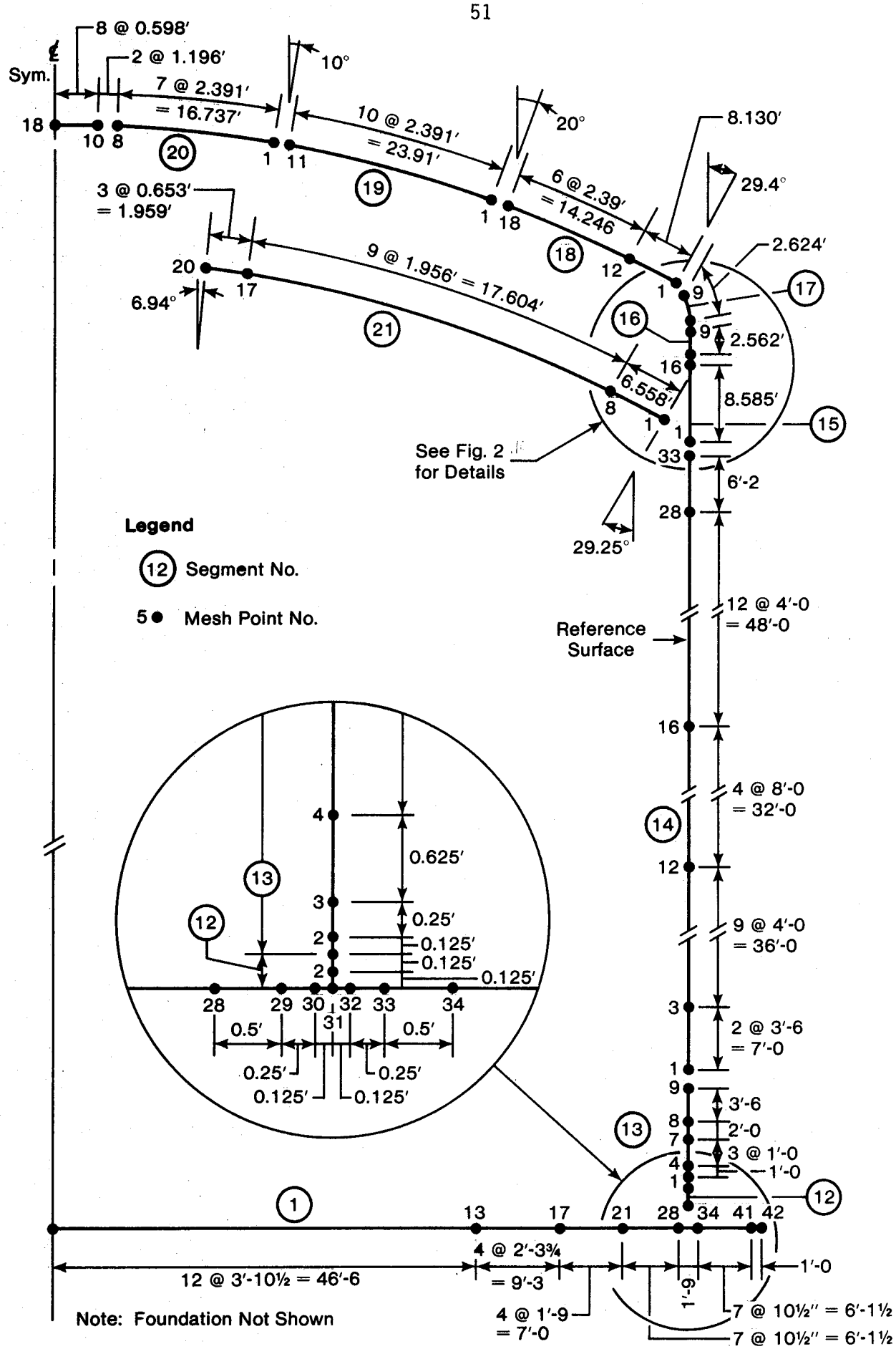

Fig. 2.8 Structural Model: Mesh Point Layout

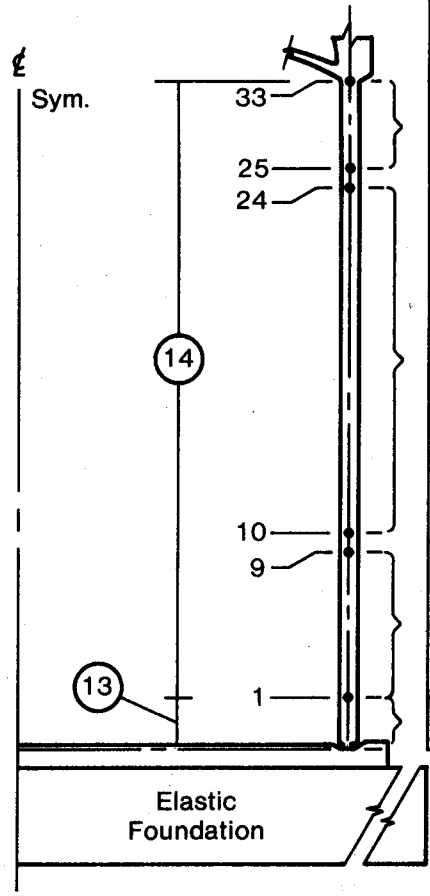

Reinforcements			
Meridional		Circumferential	
Inner Face	Outer Face	Inner Face	Outer Face
#11 @ 12″	#11 @ 12″	#11 @ 12″	#11 @ 12″
#8 @ 12″	#8 @ 12″	#7 @ 12″	#10 @ 12″
#9 @ 12″	#9 @ 12″	#10 @ 12″	#10 @ 12″
#9 @ 12″	#9 @ 12″	#11 @ 12″	#11 @ 12″ #11 @ 6″ *

*Extra Reinforcements Are Also Included for Segment 12-Refer (B)

(A) Nominal Reinforcemens

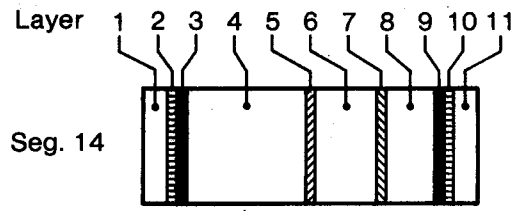

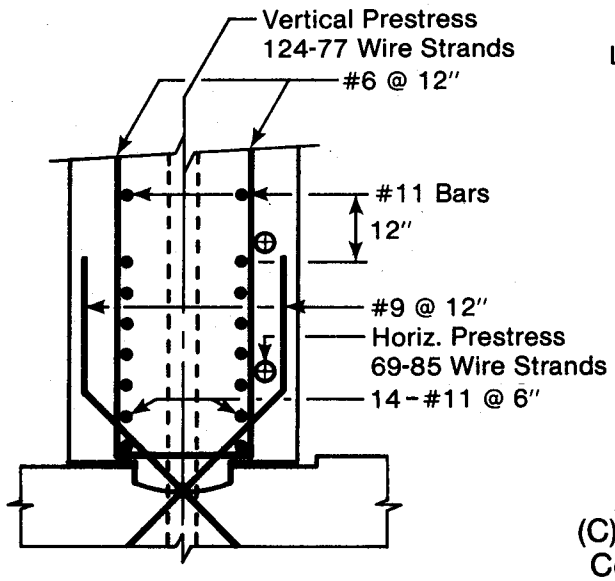

(B) Extra Reinforcements Near Base

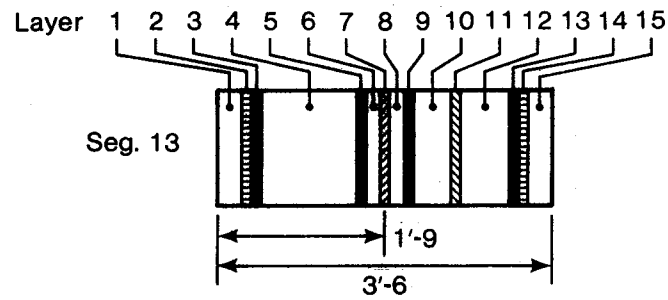

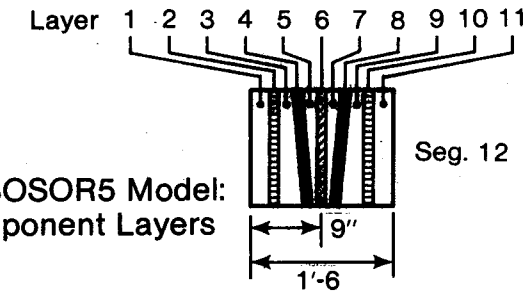

(C) BOSOR5 Model: Component Layers

Fig. 2.9 Reinforcing and Layering for Wall Segments

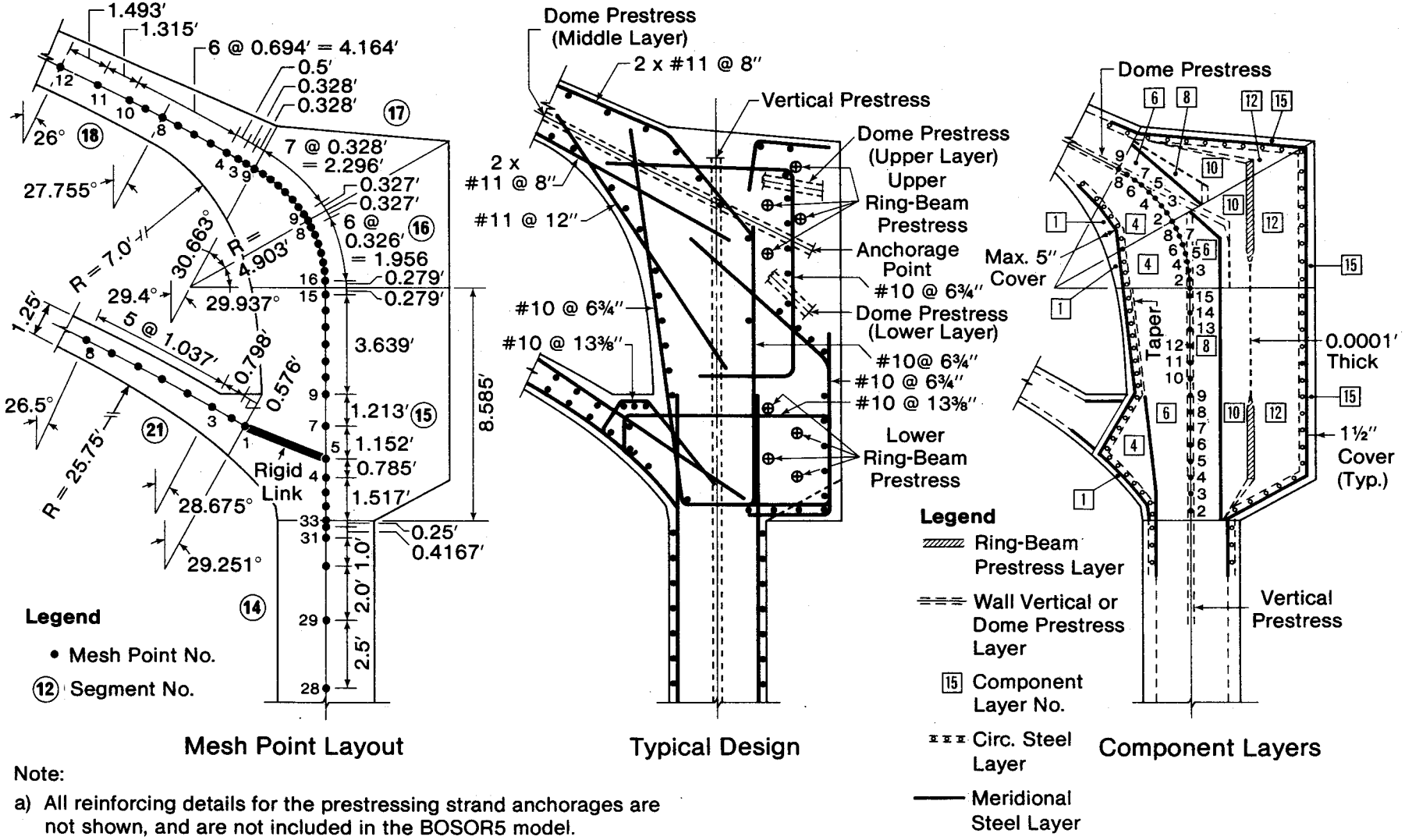

Note:

a) All reinforcing details for the prestressing strand anchorages are not shown, and are not included in the BOSOR5 model.

b) The meridional component of the dome prestressing is assumed to follow the middle layer of the 3-layer net.

c) All circumferential reinforcements are assumed to be #10 bars

Fig. 2.10 Reinforcing and Layering for Ring Beam Segments

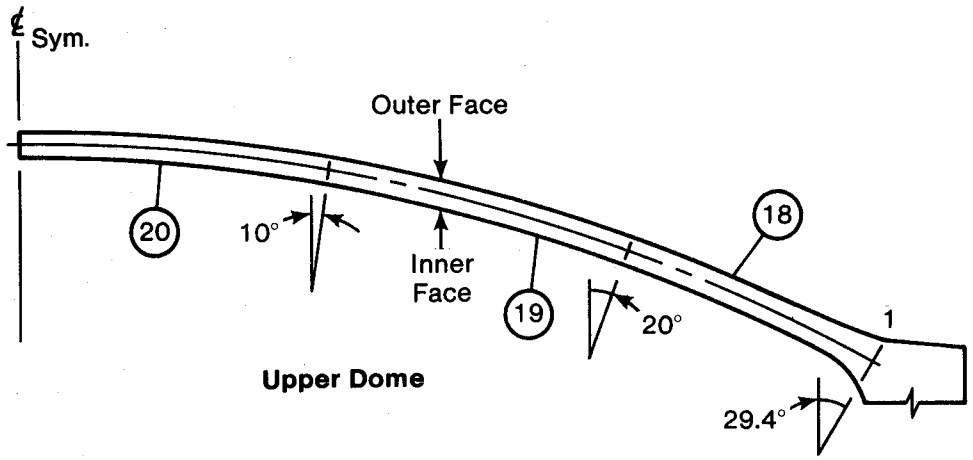

Segment	Mesh Points	Reinforcements			
		Meridional		Circumferential	
		Inner Face	Outer Face	Inner Face	Outer Face
18	1 to 13	288 #11	288 #11	#10 @ 12″	#10 @ 9″ *
	16 to 18	288 #11	288 #11	#10 @ 15″	#10 @ 15″
19	6	192 #11	216 #11	#10 @ 15″	#10 @ 15″
	7 to 9	192 #11	216 #11	#10 @ 15″	#10 @ 7½″
	9 to 11	192 #11	216 #11	#10 @ 7½″	#10 @ 7½″
20	1 to 4	192 #11	144 #11	#10 @ 7½″	#10 @ 7½″
	7 to 10	96 #11	96 #11	#10 @ 7½″	#10 @ 7½″
	10 to 14	24 #11	24 #11	#10 @ 6″	#10 @ 6″
	18	8 #11	8 #11	#10 @ 6″	#10 @ 6″

*Plus Extra Steel From Ring-Beam

Note: a) The number of bars in the meridional direction is for the entire dome

b) The steel areas for the intermediate points are linearly interpolated.

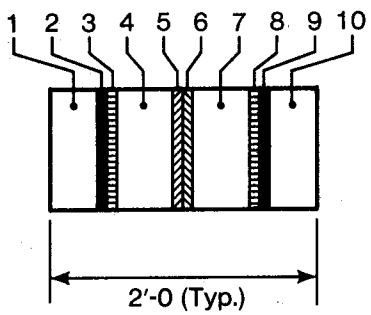

Component Layers

Fig. 2.11 Reinforcing and Layering for Upper Dome Segments

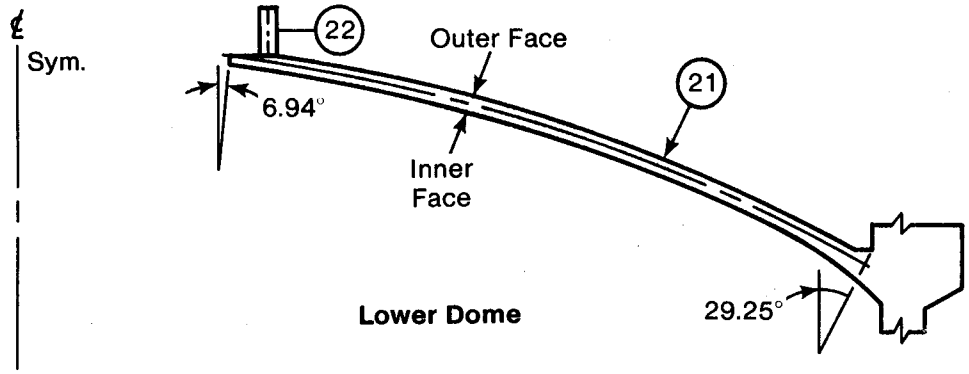

Segment	Mesh Points	Reinforcements			
		Meridional		Circumferential	
		Inner Face	Outer Face	Inner Face	Outer Face
21	1 to 8	208 #10 624 #8	416 #10	#10 @ 15½"	#10 @ 15½" *
	10 to 14	416 #10	416 #10	#10 @ 15½"	#10 @ 15½"
	16 to 17	208 #10	208 #10	#10 @ 15½"	#10 @ 15½"
	20	208 #4	208 #4	#10 @ 15½"	#10 @ 15½"
22	1 to 3	#6 @ 9"	#6 @ 9"	#8 @ 8"	#8 @ 8"

*Plus Extra Steel From Ring-Beam

Note: a) The number of bars in the meriodional directions is for the entire dome.

Note: b) The steel areas for intermediate points are linearly interpolated

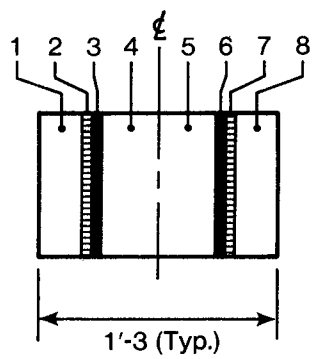

Component Layers

Fig. 2.12 Reinforcing and Layering for Lower Dome Segments

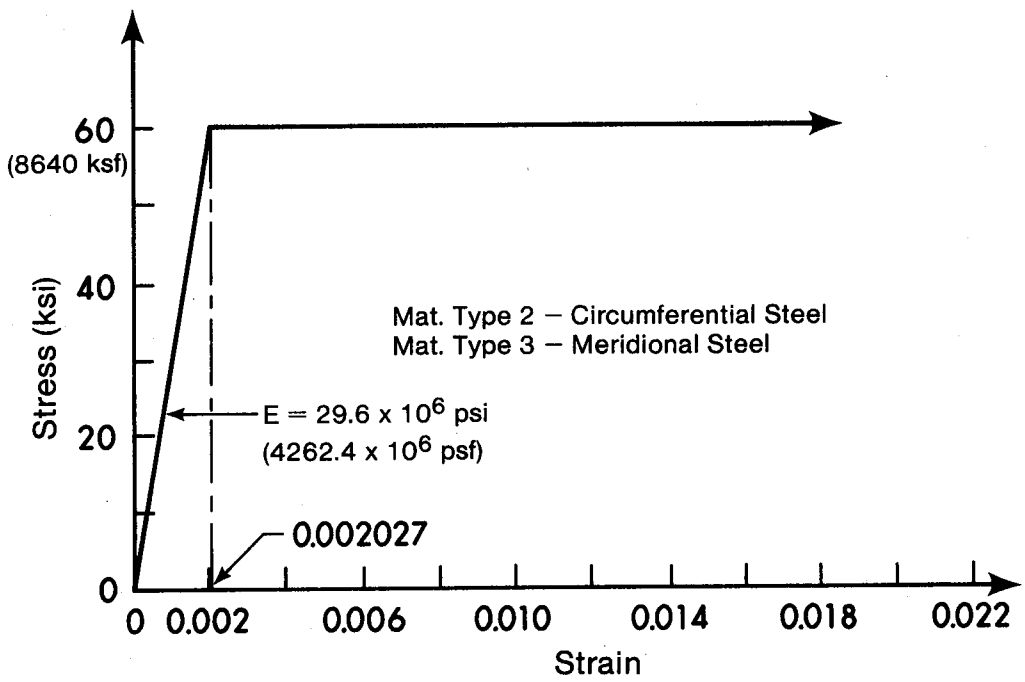

Fig. 2.13 Stress-Strain for Reinforcing Bars

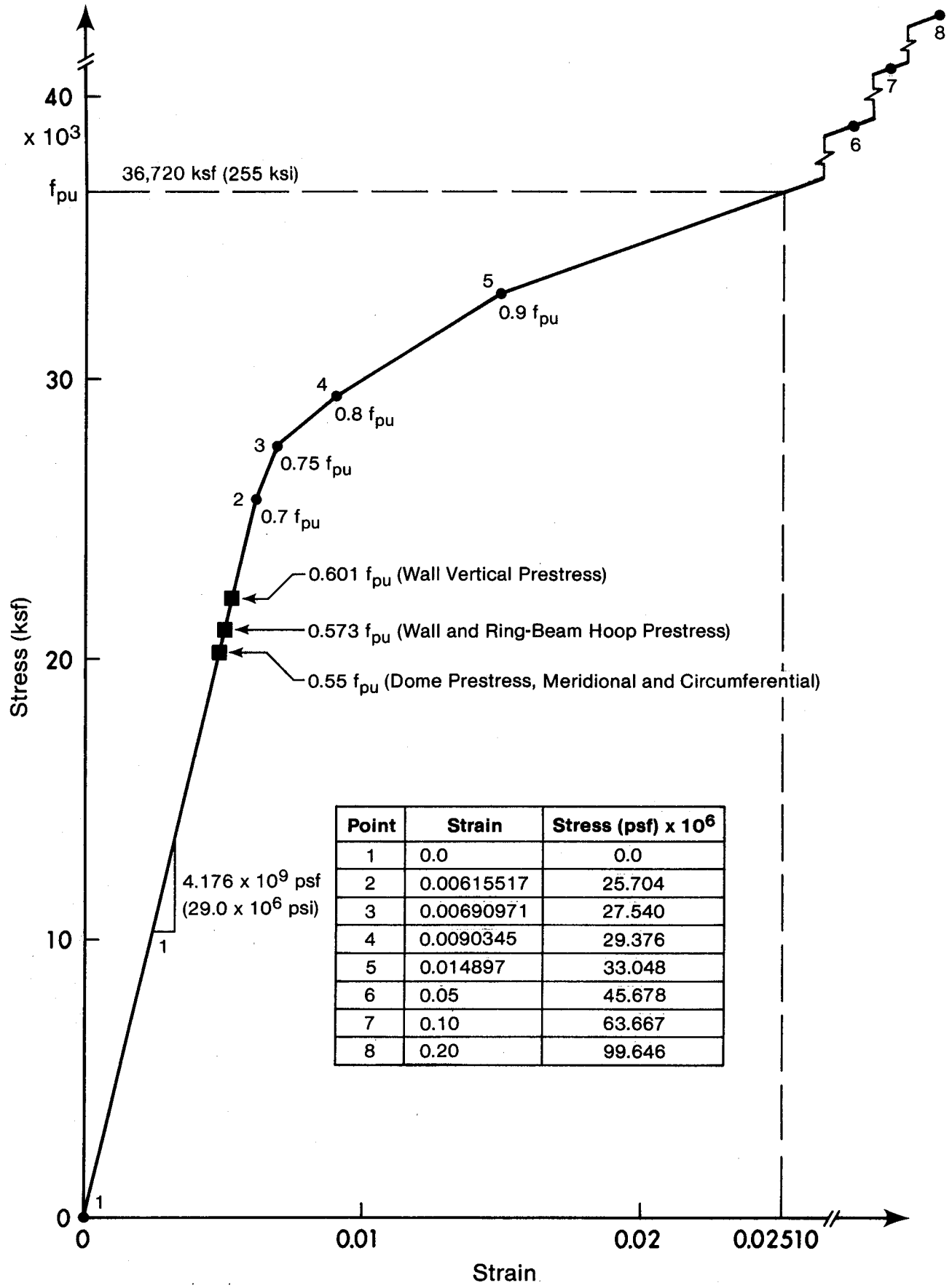

Point	Strain	Stress (psf) x 10^6
1	0.0	0.0
2	0.00615517	25.704
3	0.00690971	27.540
4	0.0090345	29.376
5	0.014897	33.048
6	0.05	45.678
7	0.10	63.667
8	0.20	99.646

Fig. 2.14 Stress-Strain for Prestressing Cables

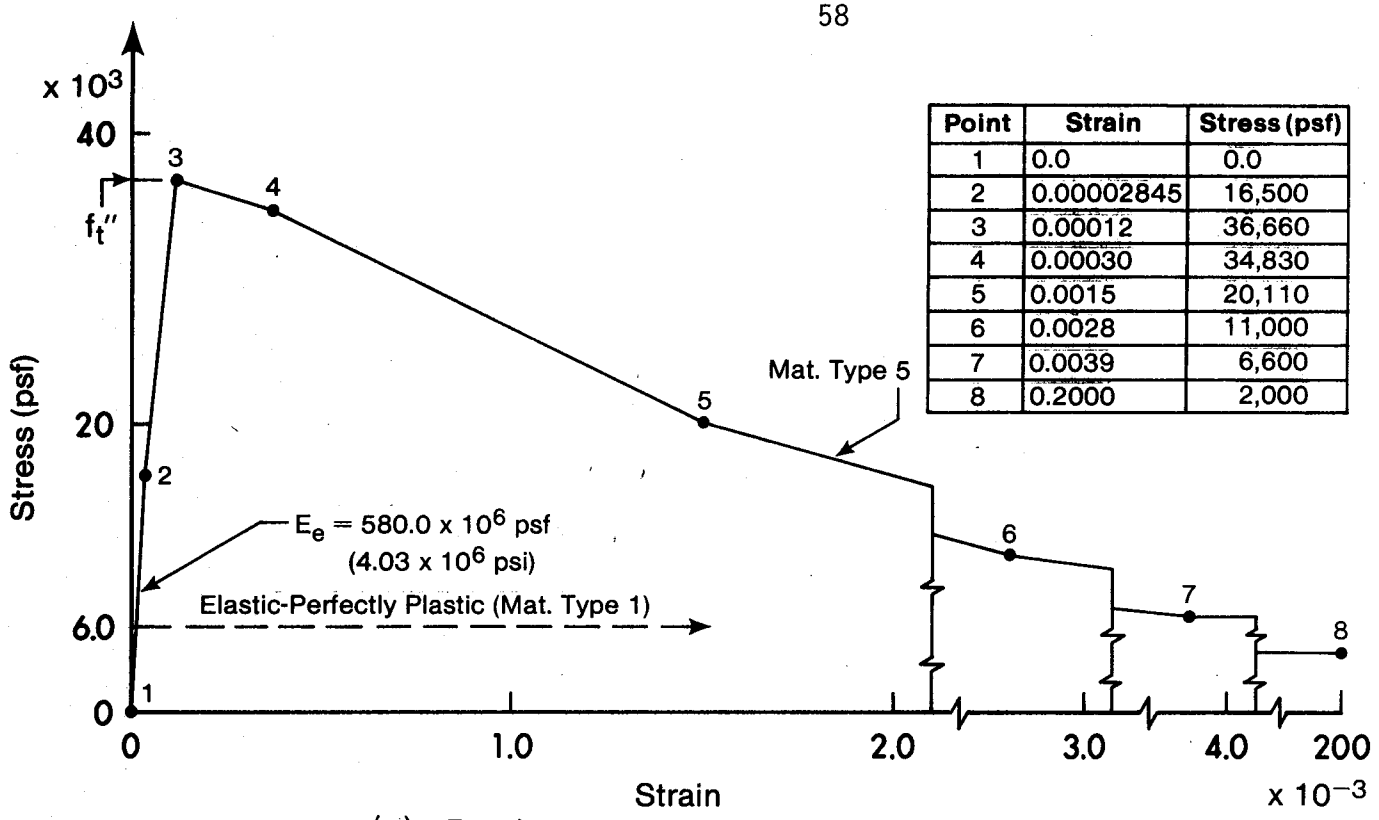

Point	Strain	Stress (psf)
1	0.0	0.0
2	0.00002845	16,500
3	0.00012	36,660
4	0.00030	34,830
5	0.0015	20,110
6	0.0028	11,000
7	0.0039	6,600
8	0.2000	2,000

(a) Tension

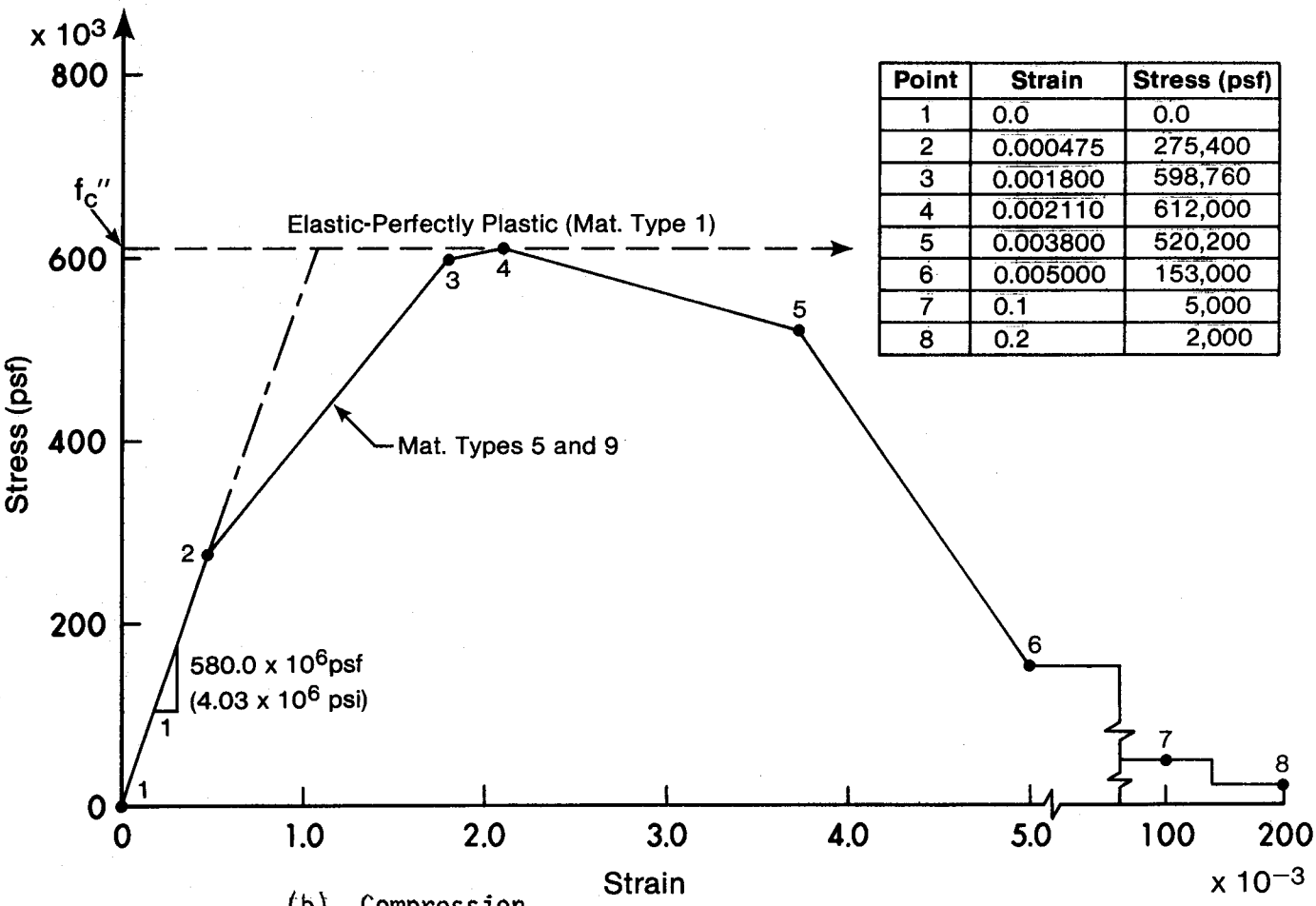

Point	Strain	Stress (psf)
1	0.0	0.0
2	0.000475	275,400
3	0.001800	598,760
4	0.002110	612,000
5	0.003800	520,200
6	0.005000	153,000
7	0.1	5,000
8	0.2	2,000

(b) Compression

Fig. 2.15 Concrete Stress-Strain: Prestressed Concrete

Point	Strain	Stress (psf)
1	0.0	0.0
2	0.0000142	8,244
3	0.00012	18,320
4	0.00030	17,400
5	0.0015	10,050
6	0.0028	5,491
7	0.0039	3,924
8	0.2000	2,000

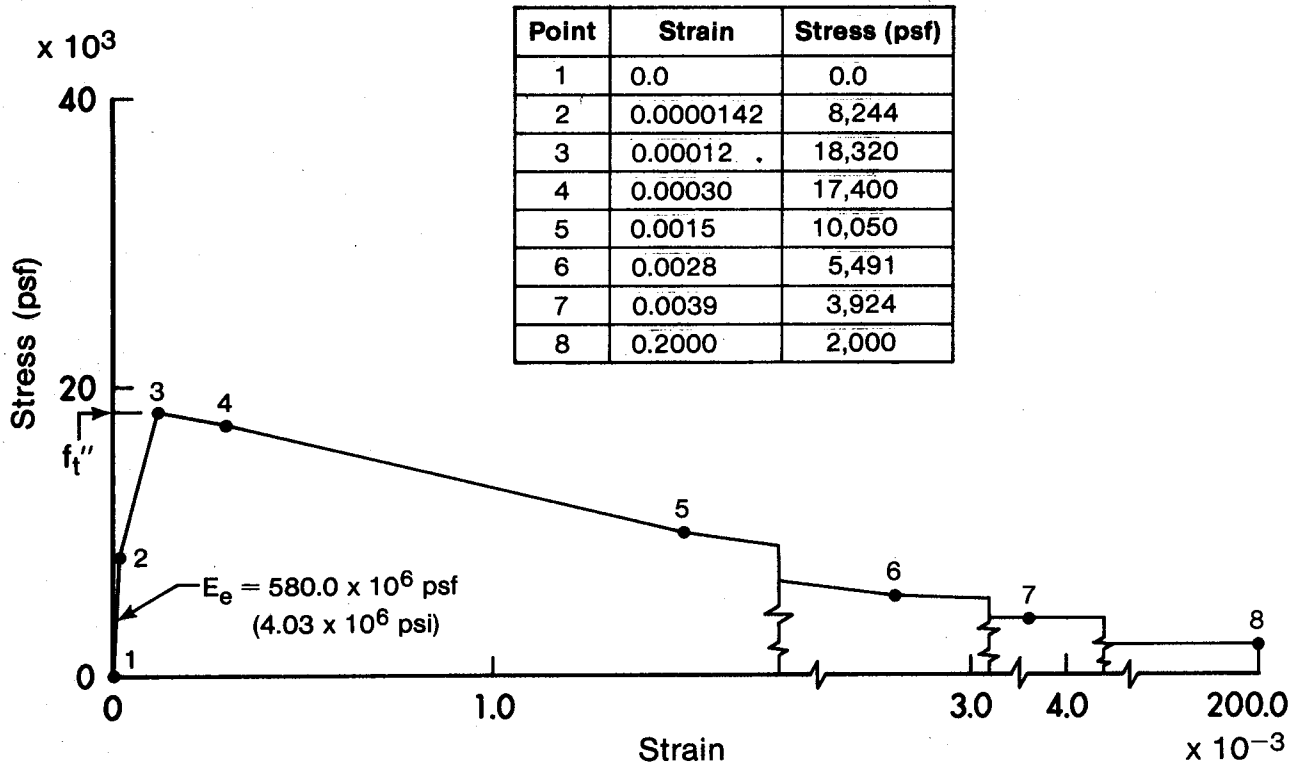

Fig. 2.16 Tensile Stress-Strain: Reinforced Concrete

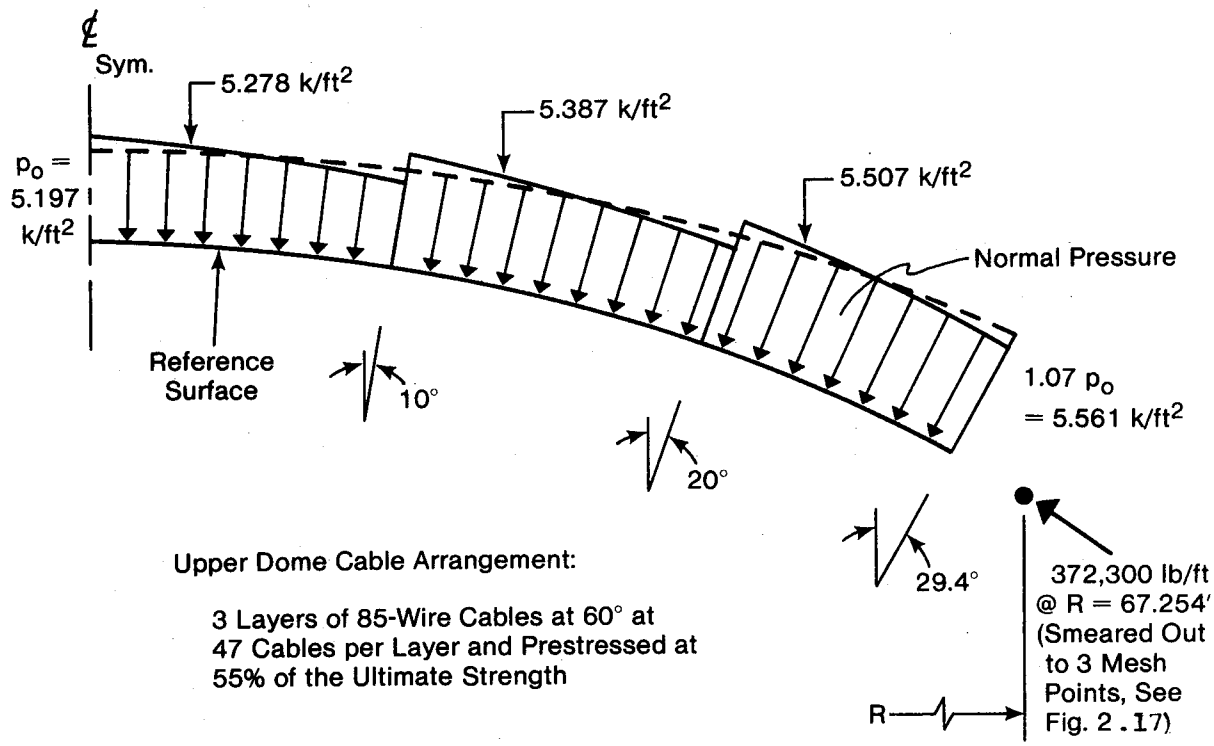

Fig. 2.18 Upper Dome Prestressing Loads

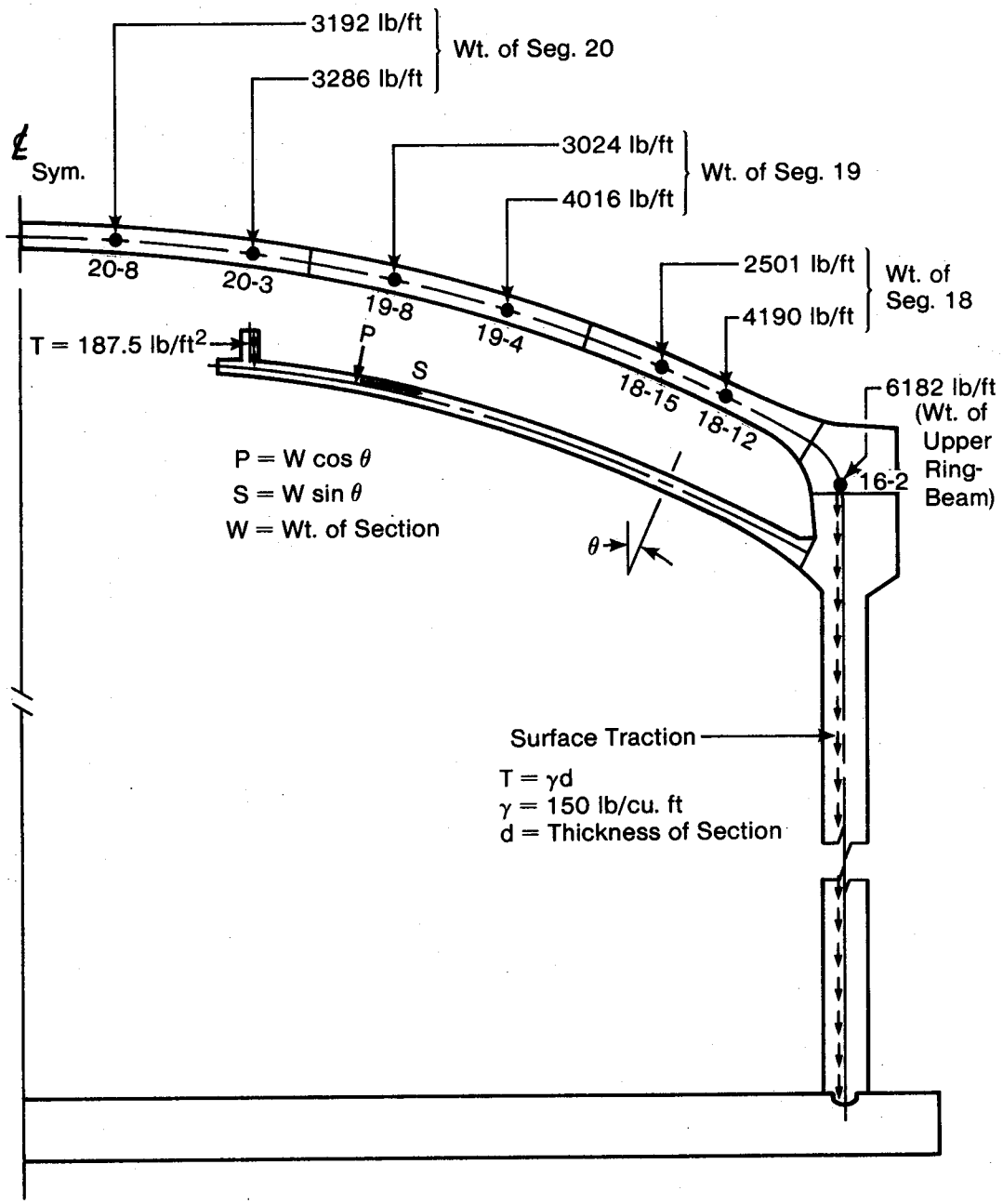

Fig. 2.19 Gravity Loads

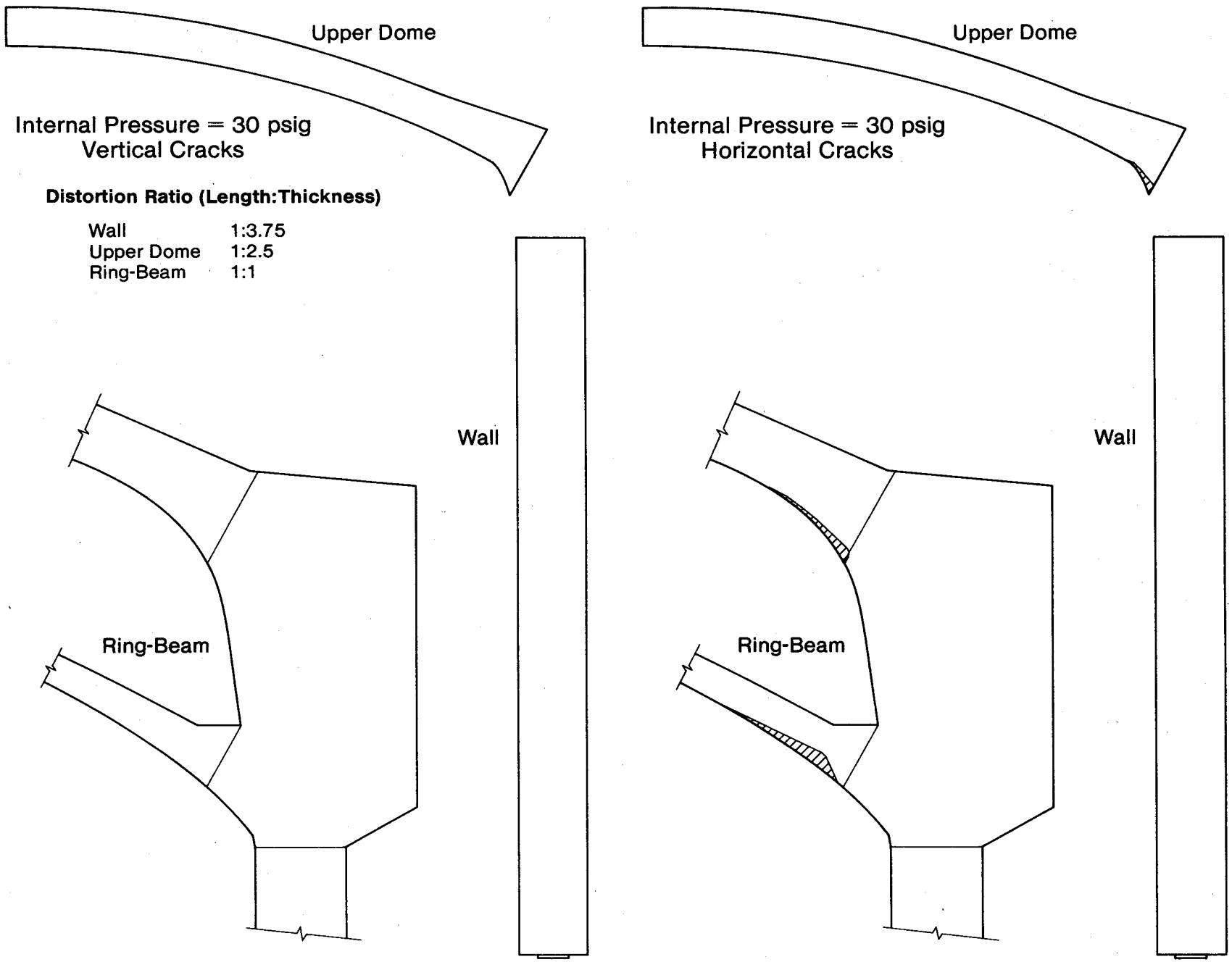

Fig. 3.1 Distribution of Cracking at 30 psi

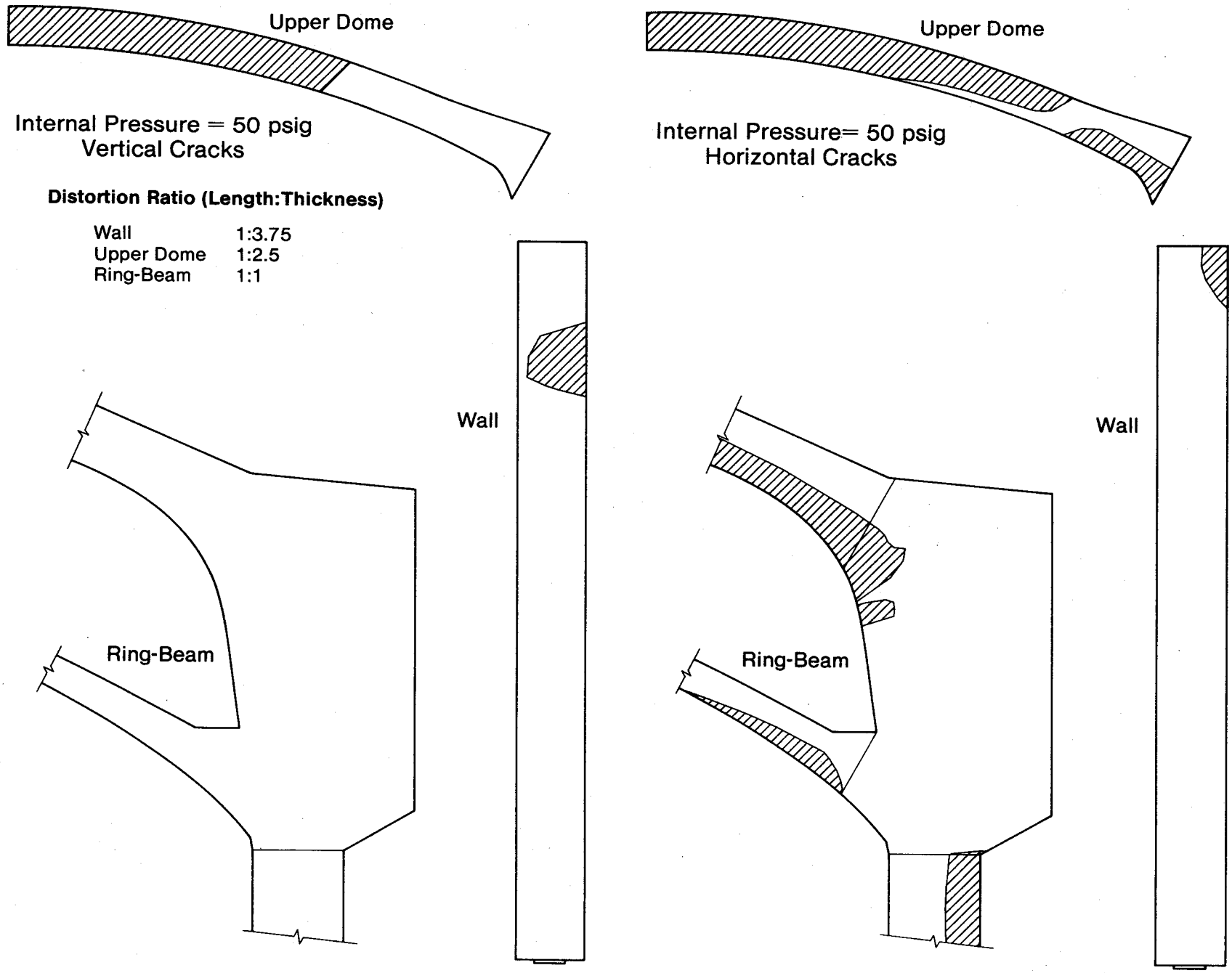

Fig. 3.2 Distribution of Cracking at 50 psi

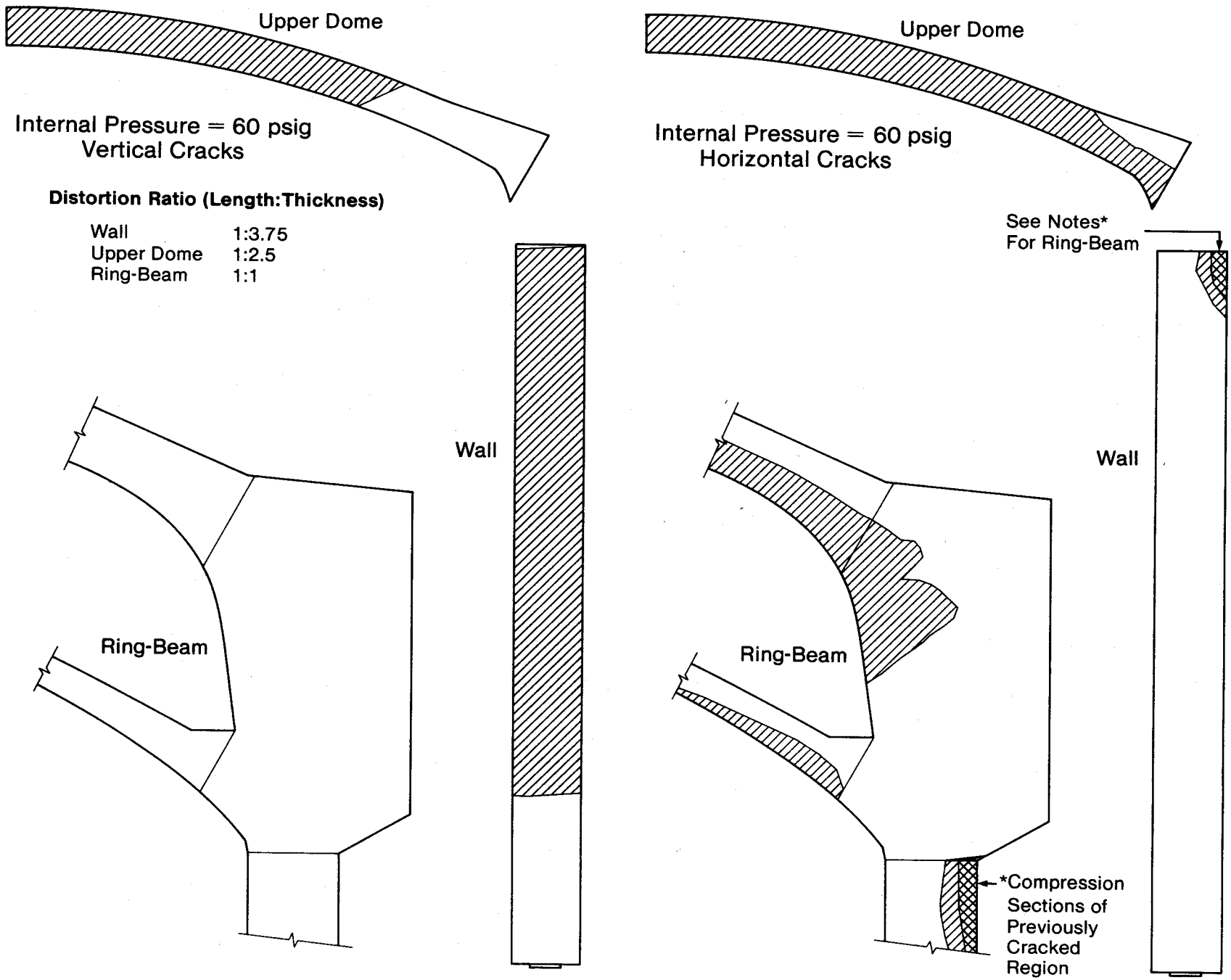

Fig. 3.3 Distribution of Cracking at 60 psi

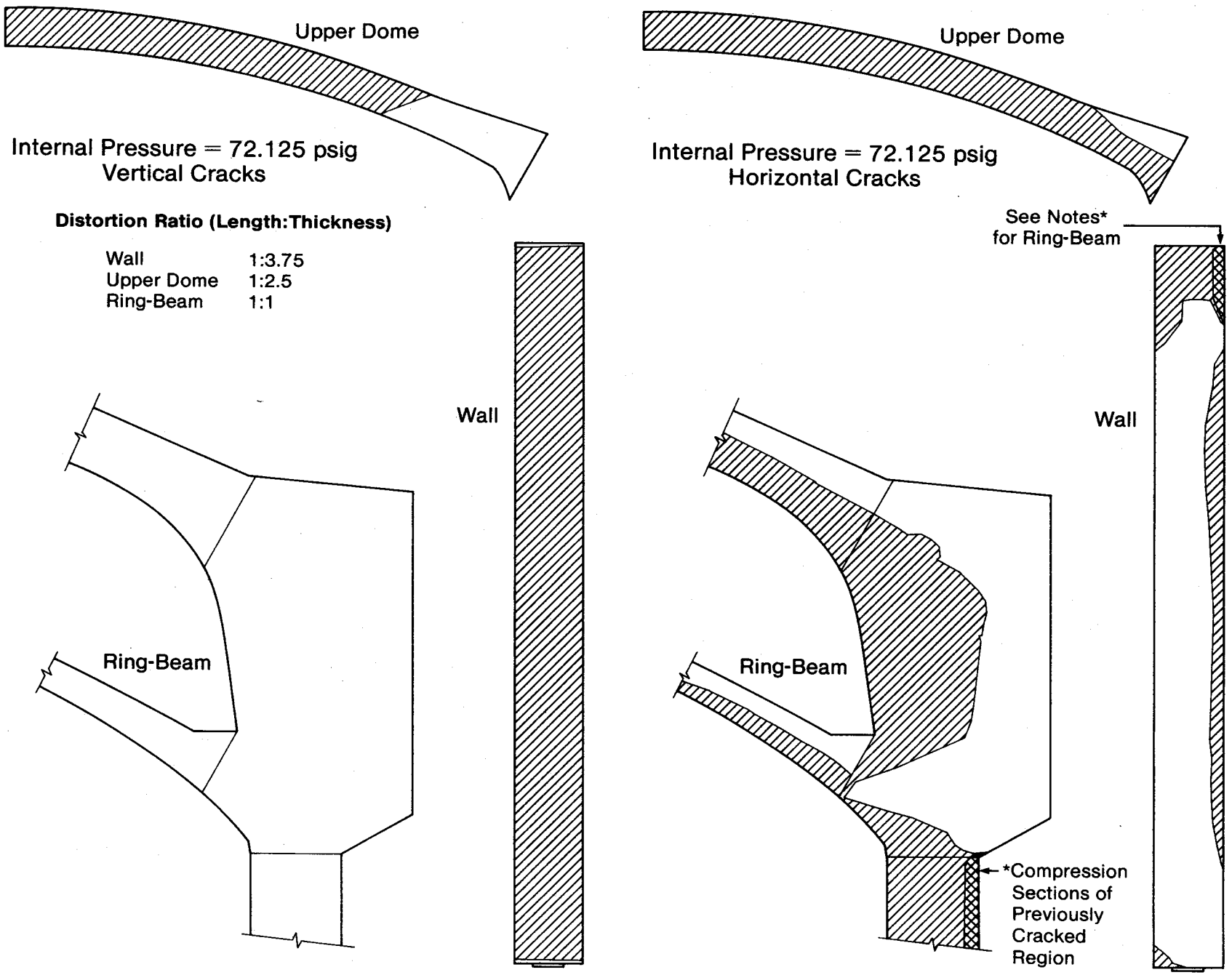

Fig. 3.4 Distribution of Cracking at 72.1 psi

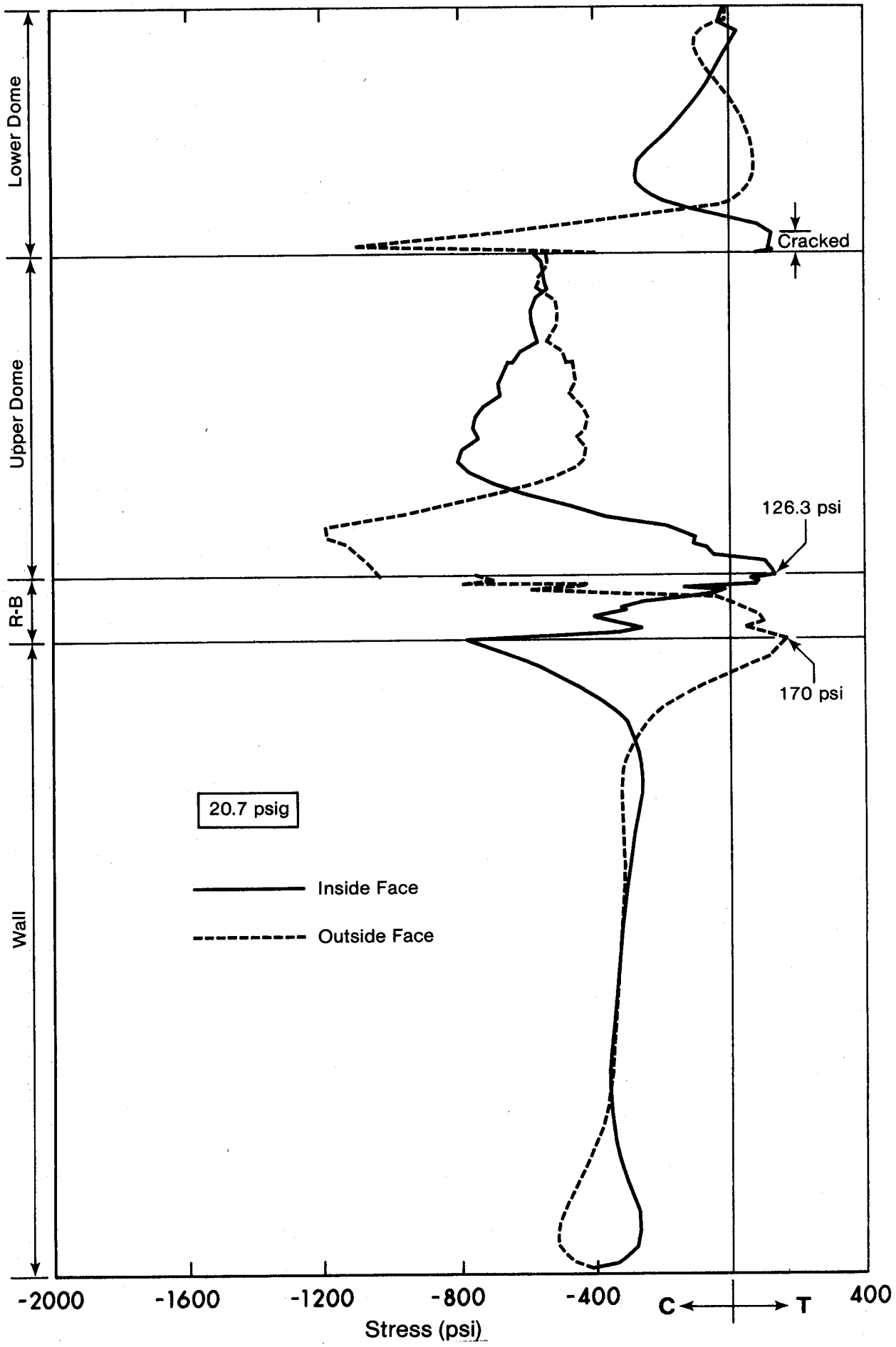

Fig. 3.5 Meridional Surface Stresses at Proof Pressure

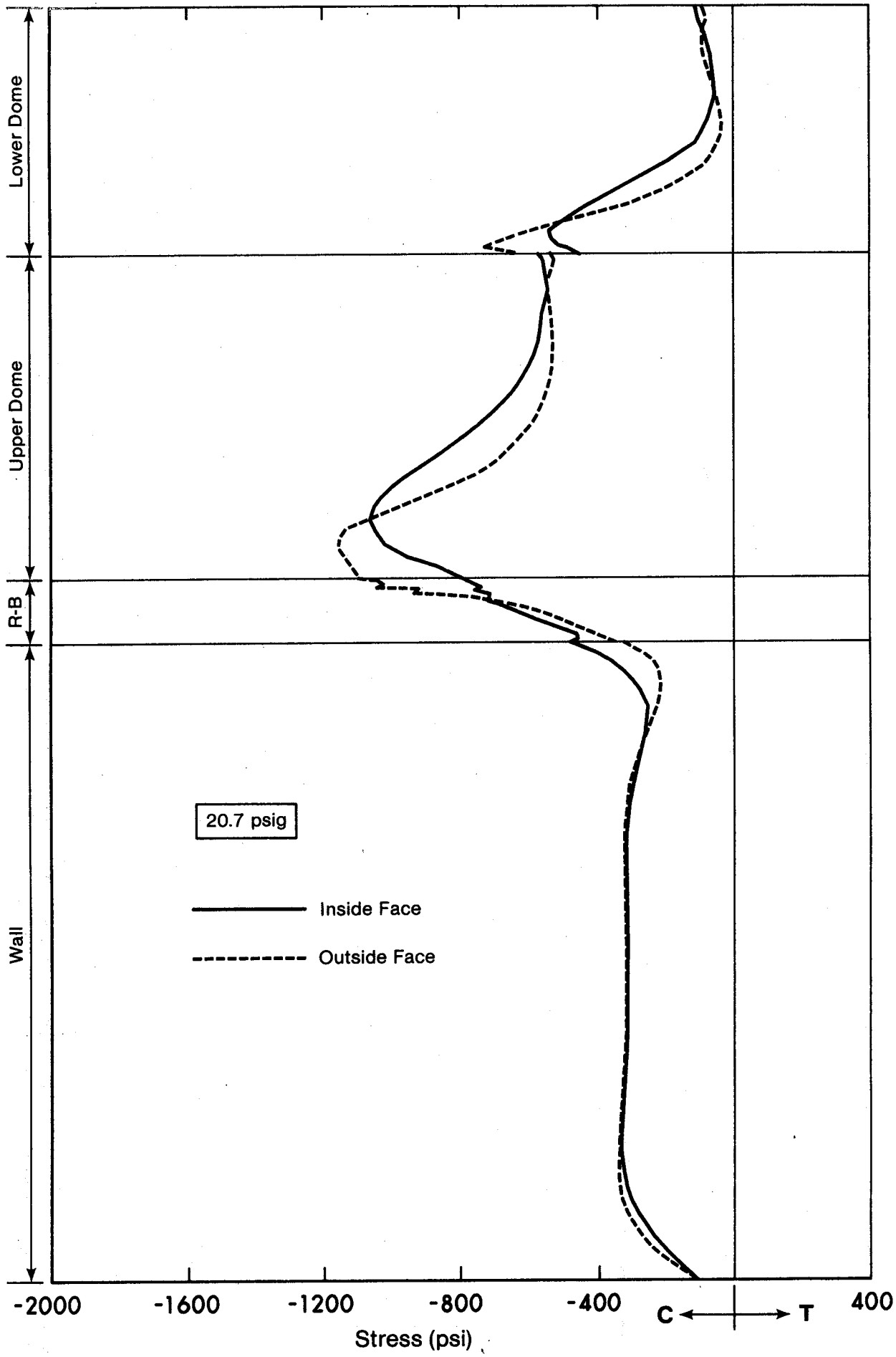

Fig. 3.6 Circumferential Surface Stresses at Proof Pressure

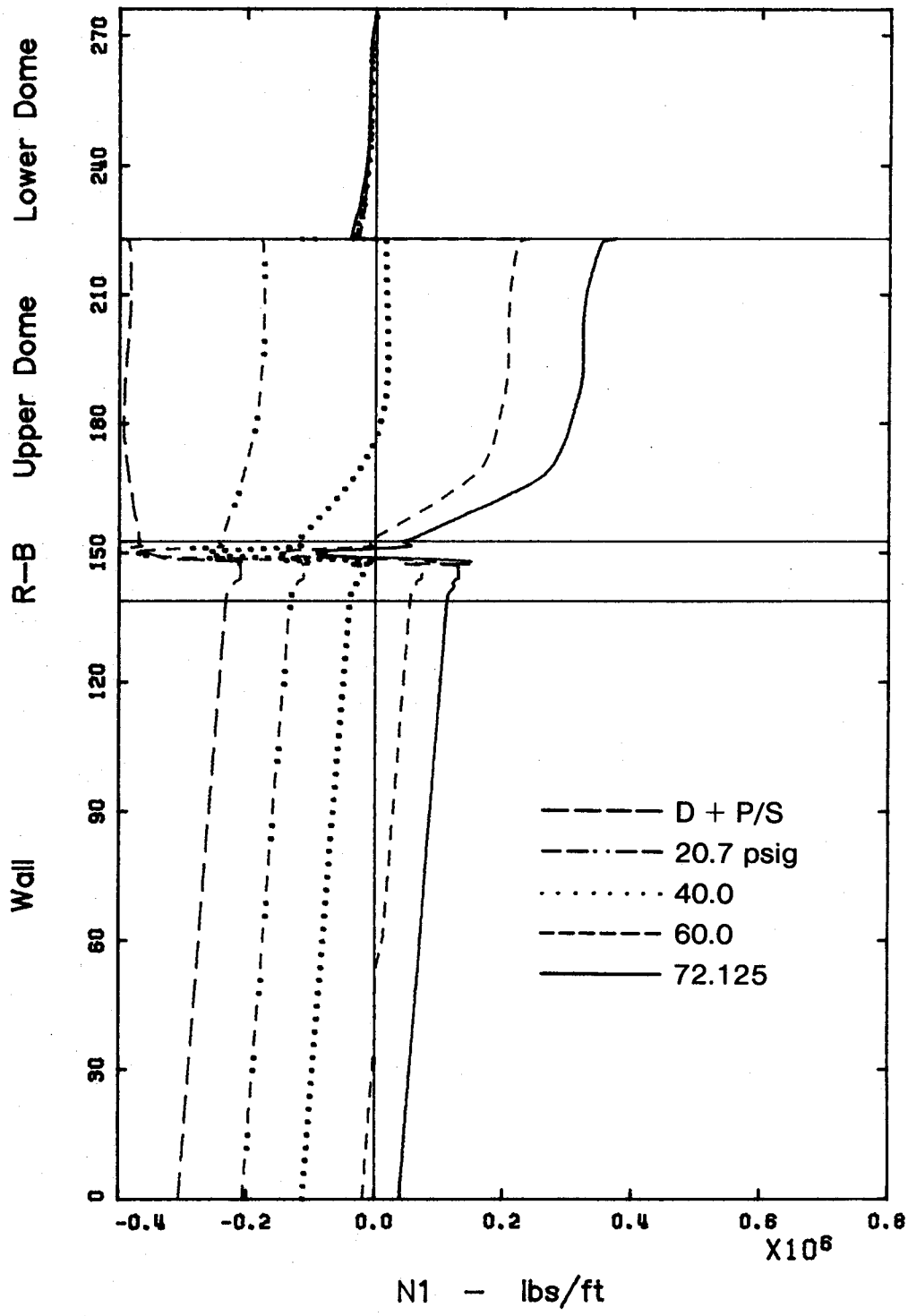

Fig. 3.7 Variation of N1 Stress Resultant

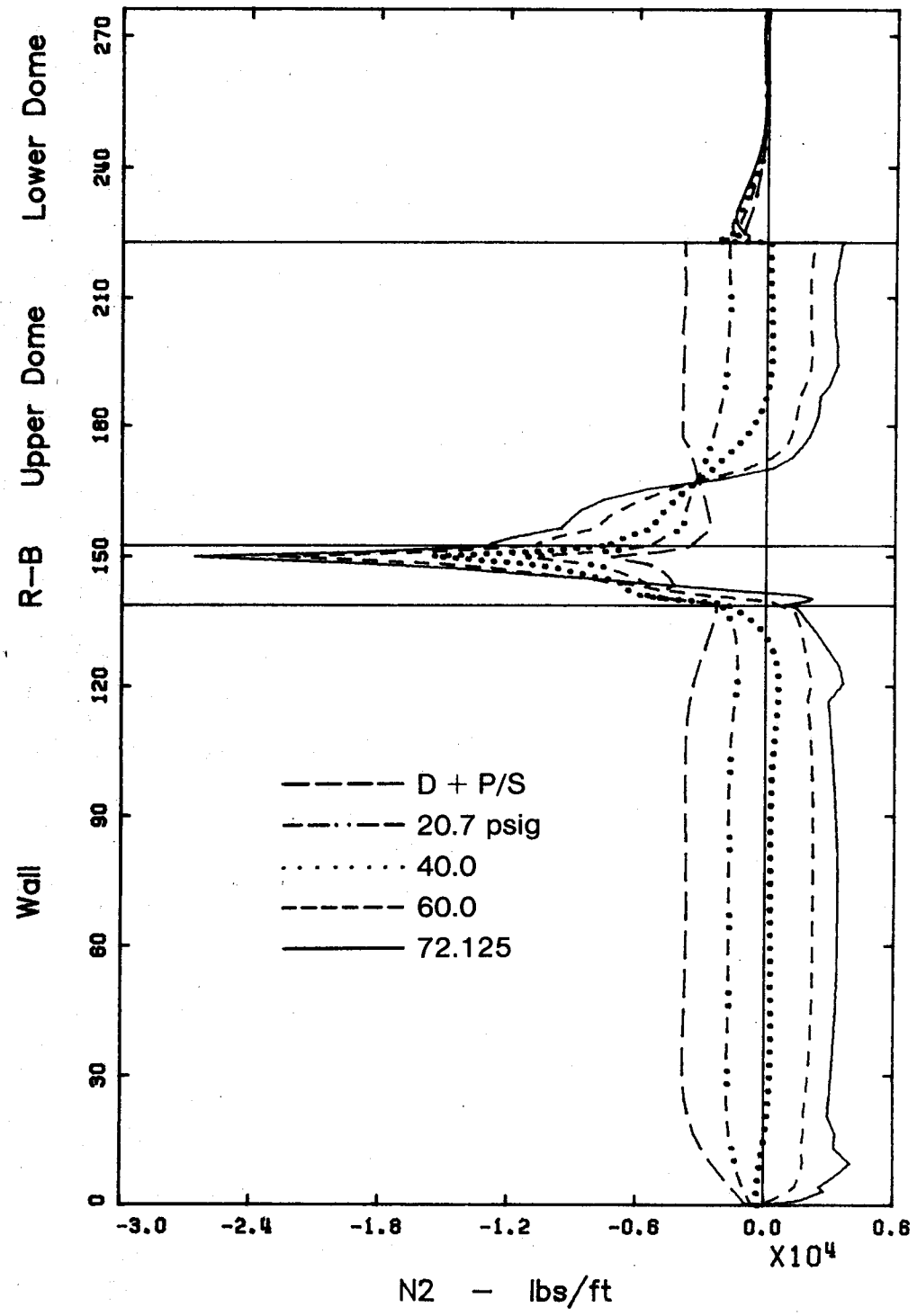

Fig. 3.8 Variation of N2 Stress Resultant

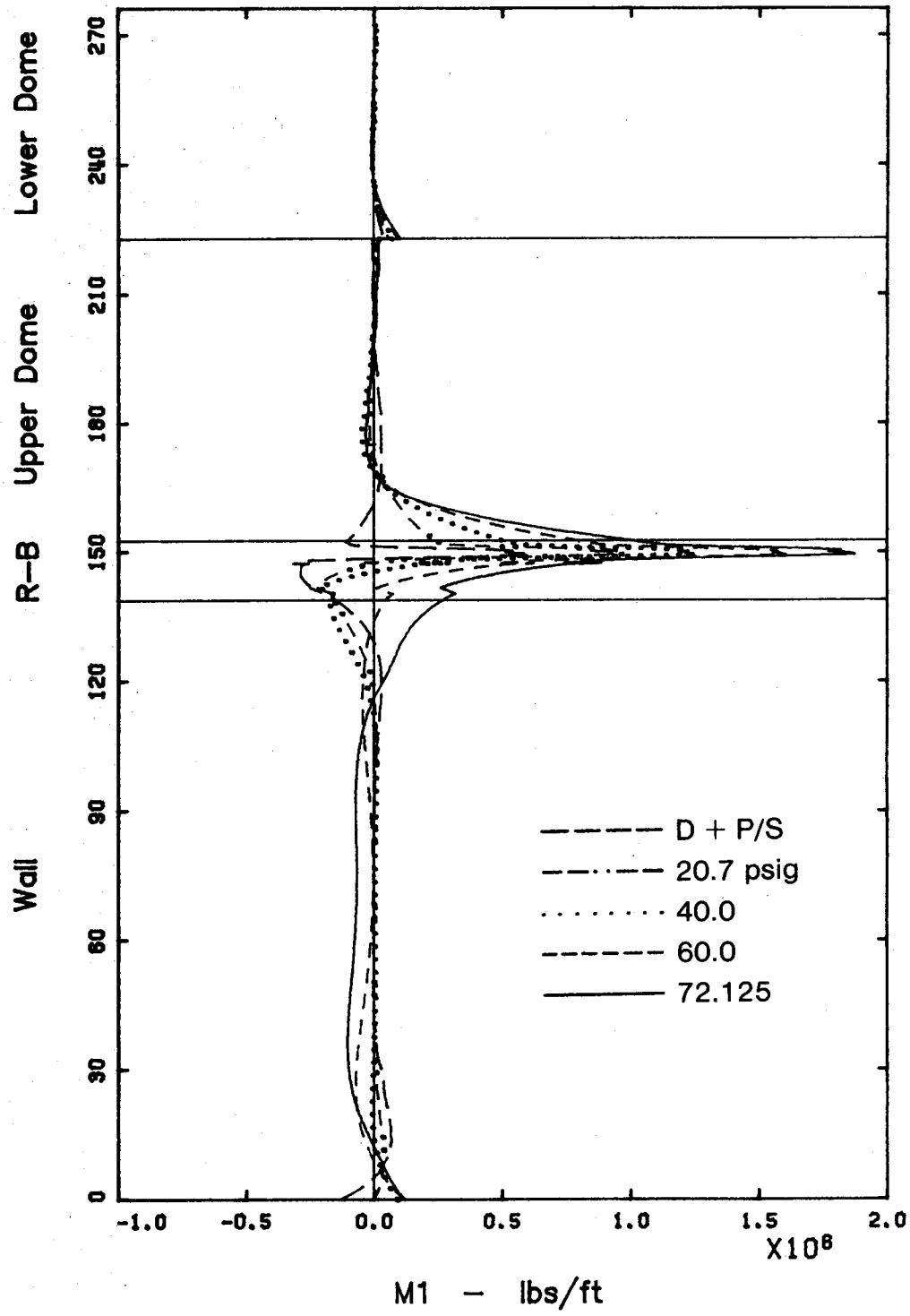

Fig. 3.9 Variation of M1 Stress Resultant

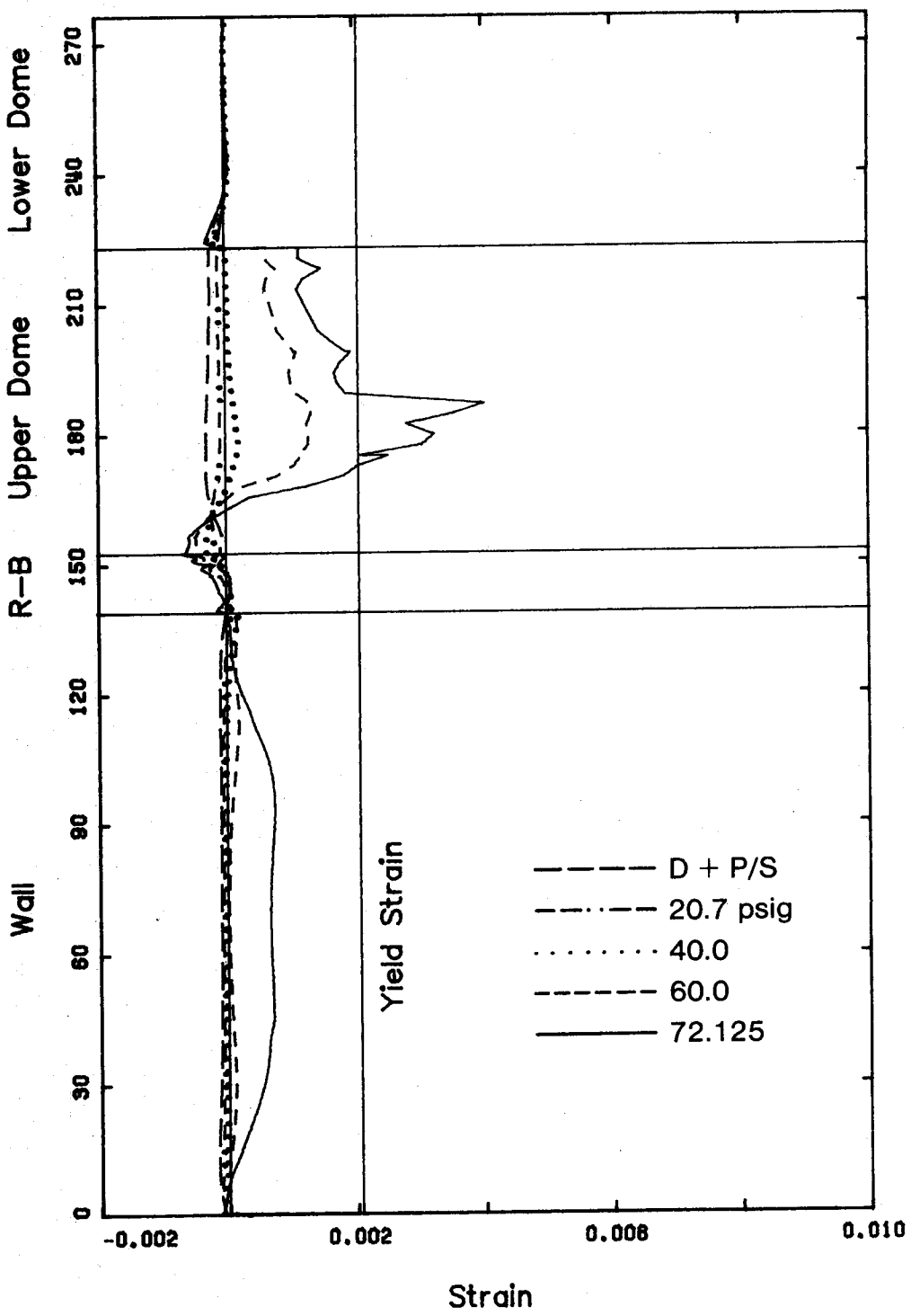

Fig. 3.10 Meridional Steel Strain: Outer Layer

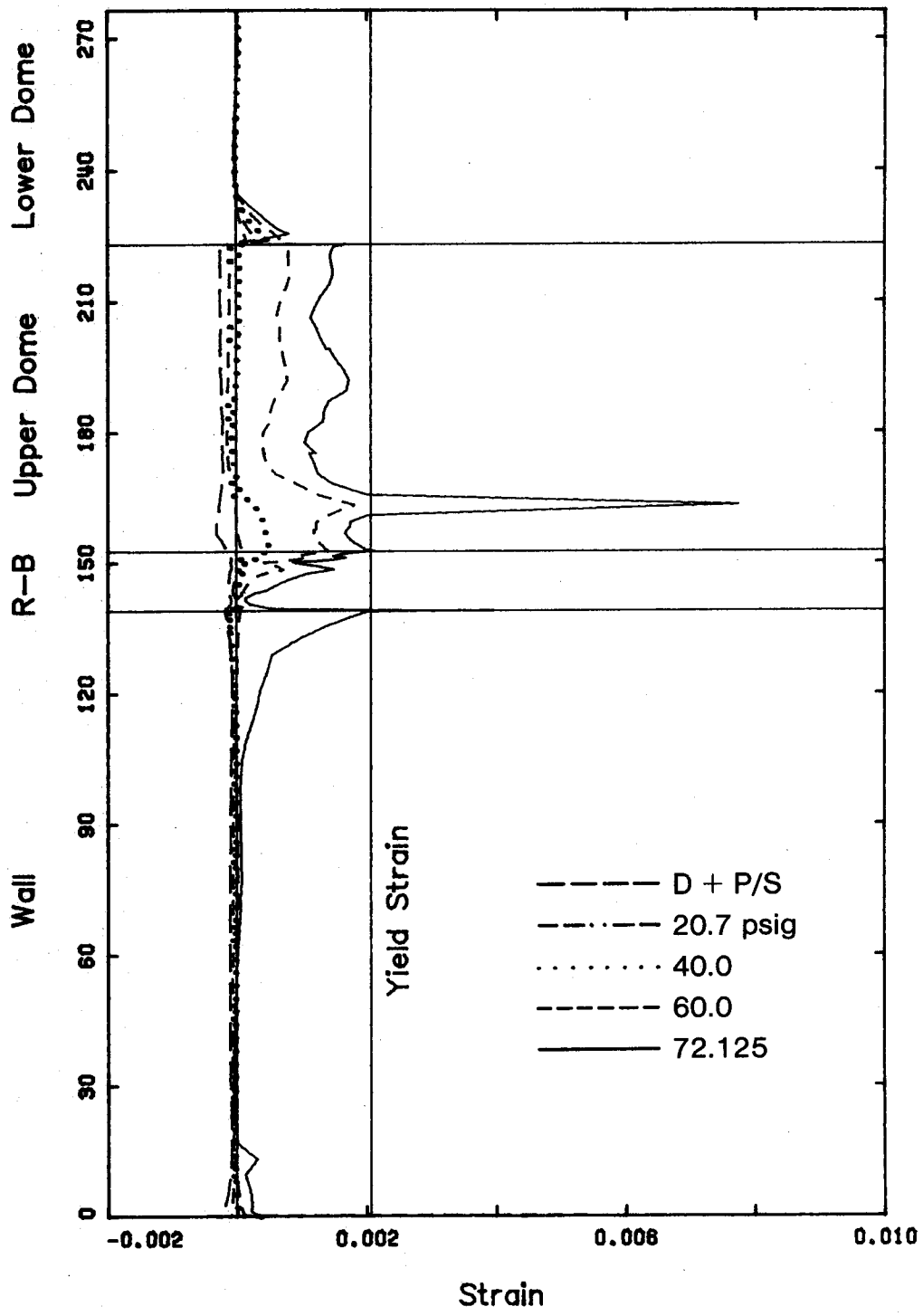

Fig. 3.11 Meridional Steel Strain: Inner Layer

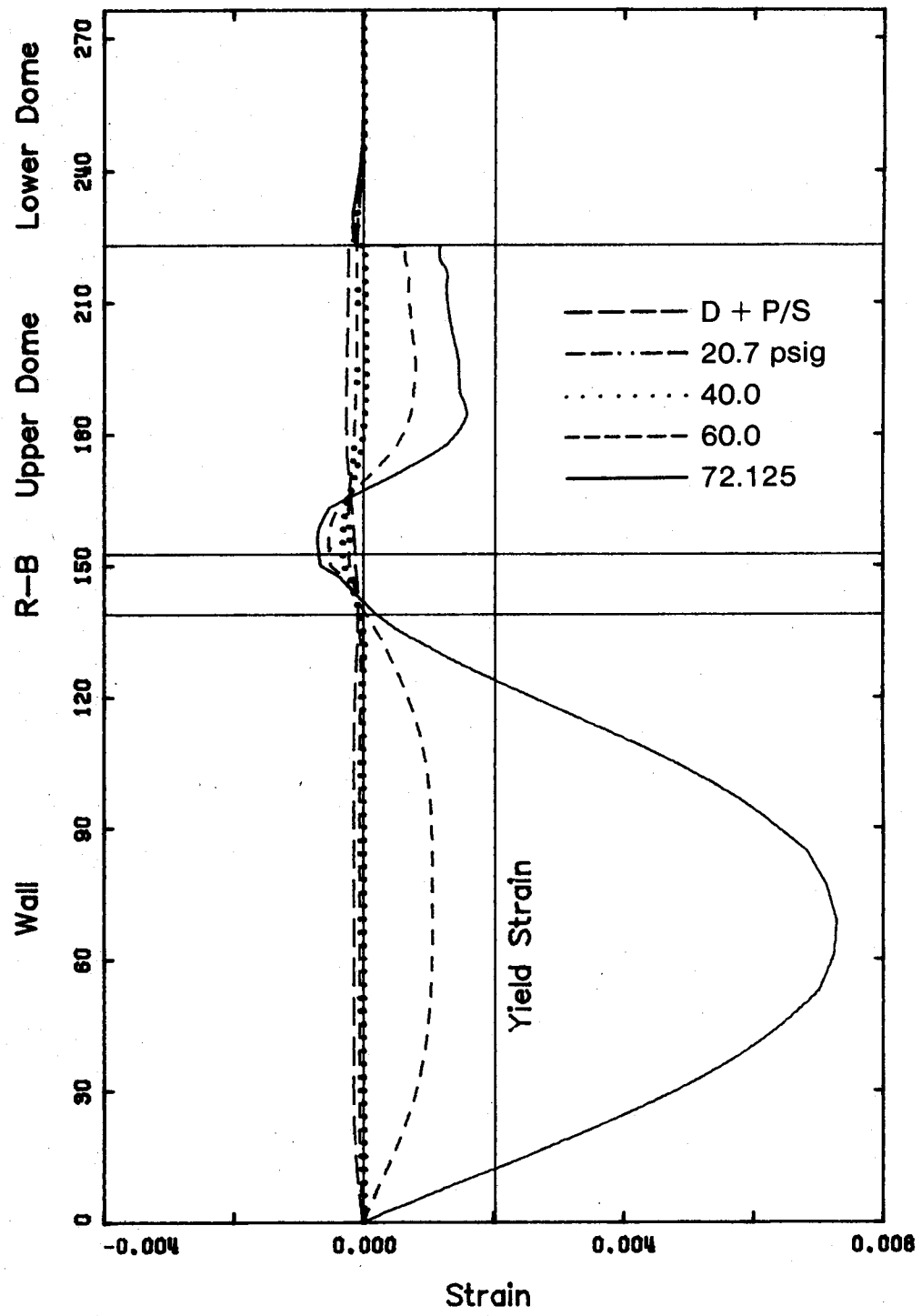

Fig. 3.12 Circumferential Steel Strain: Outer Layer

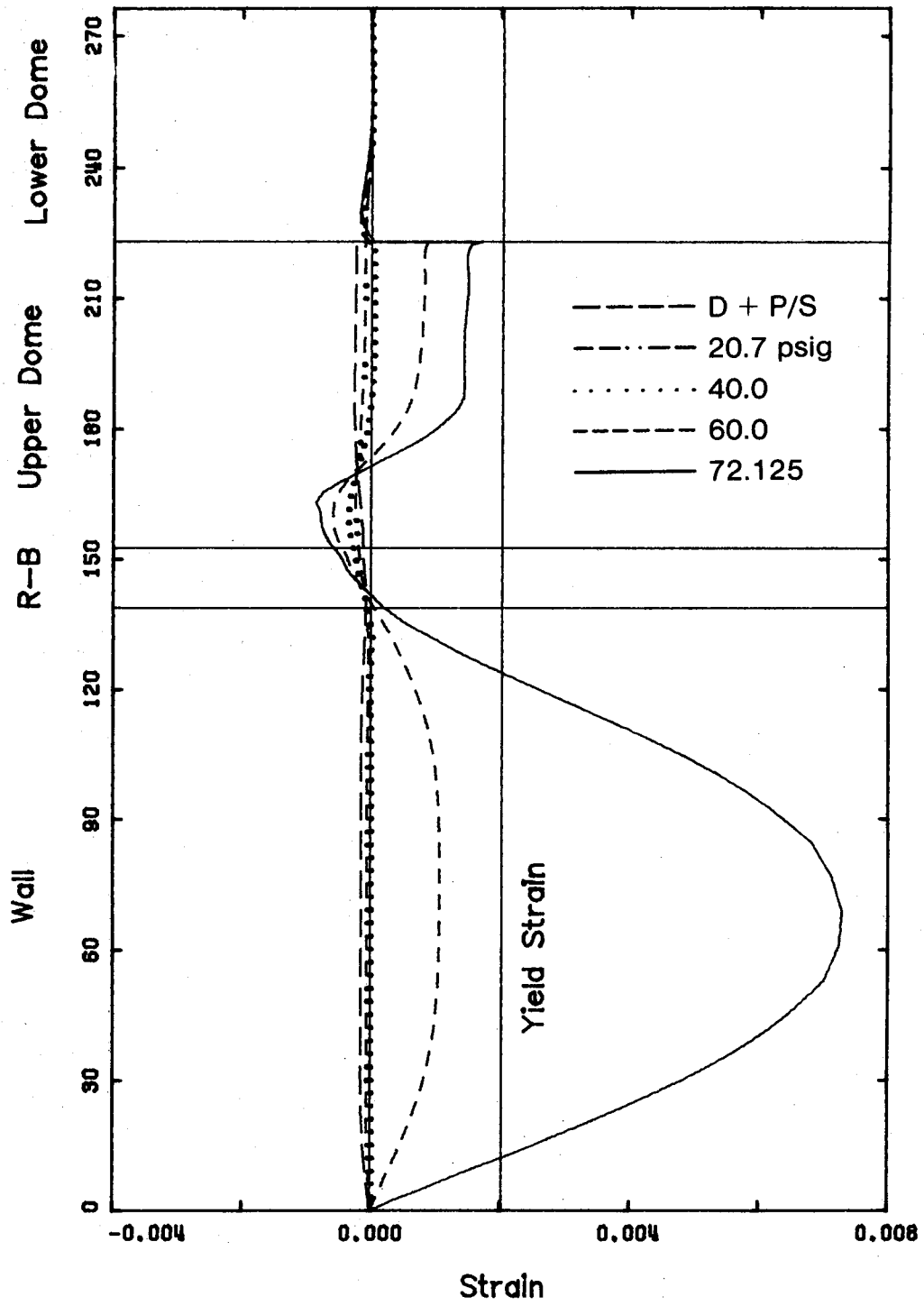

Fig. 3.13 Circumferential Steel Strain: Inner Layer

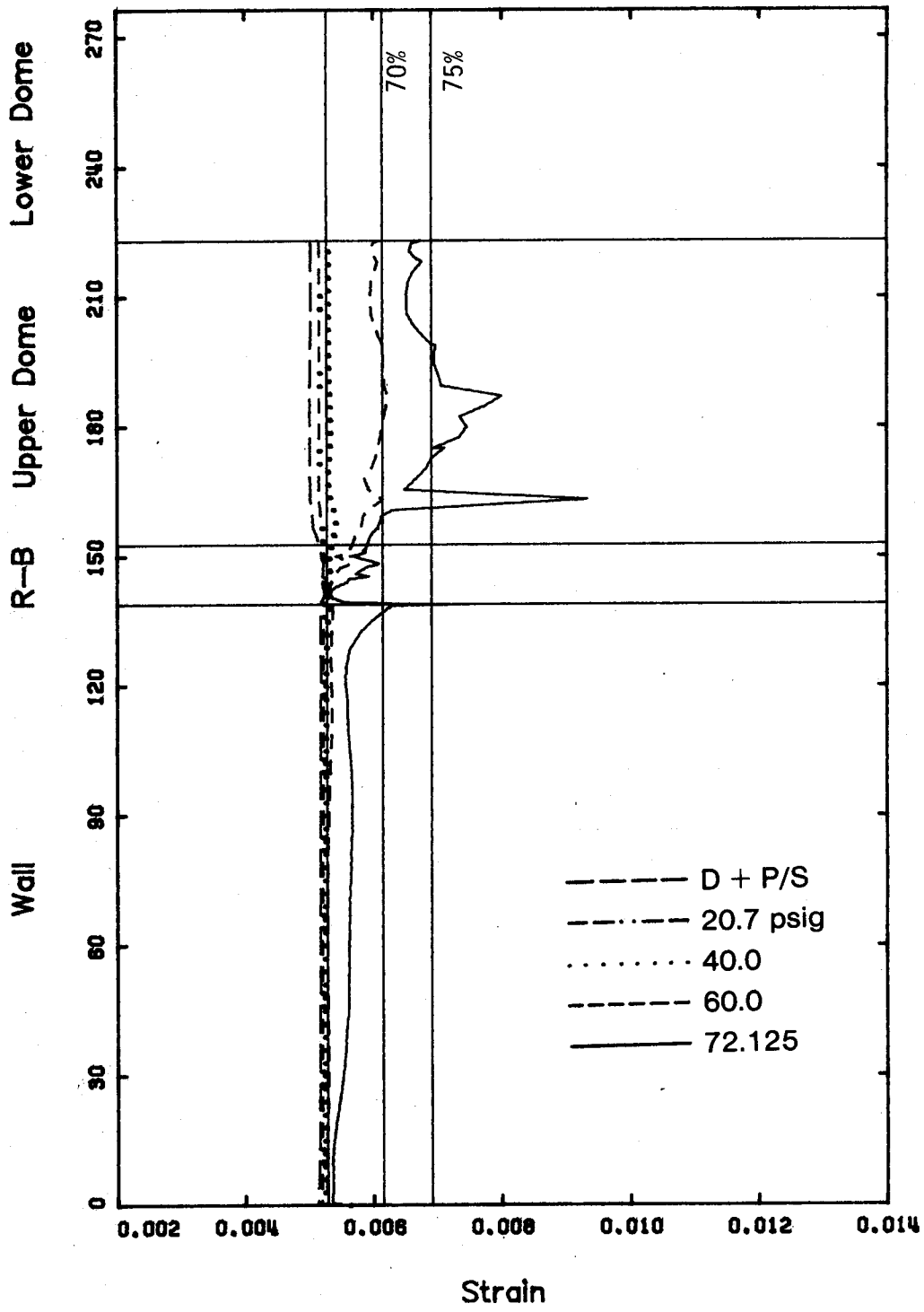

Fig. 3.14 Strain in Meridional Prestressing Cables

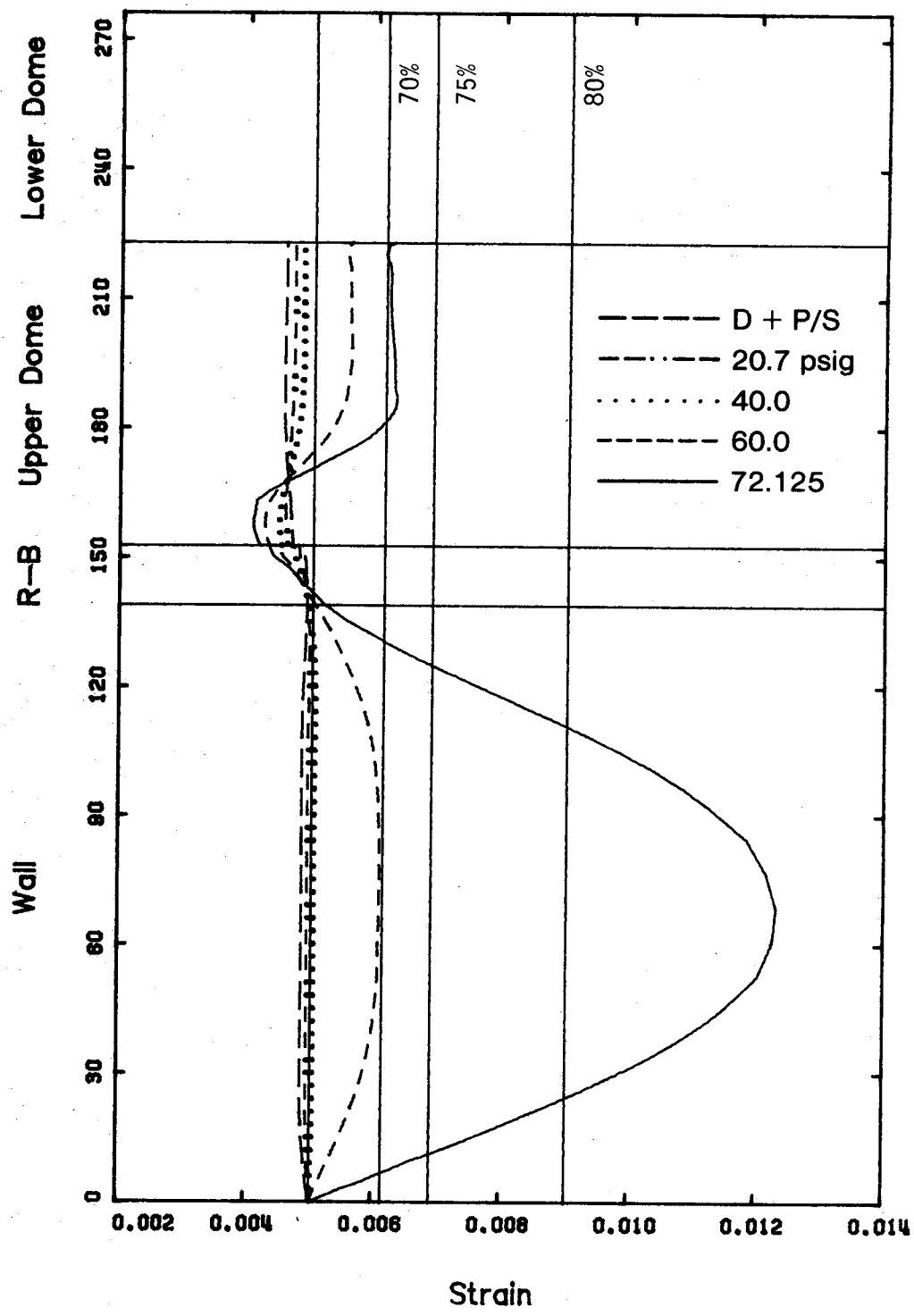

Fig. 3.15 Strain in Circumferential Prestressing Cables

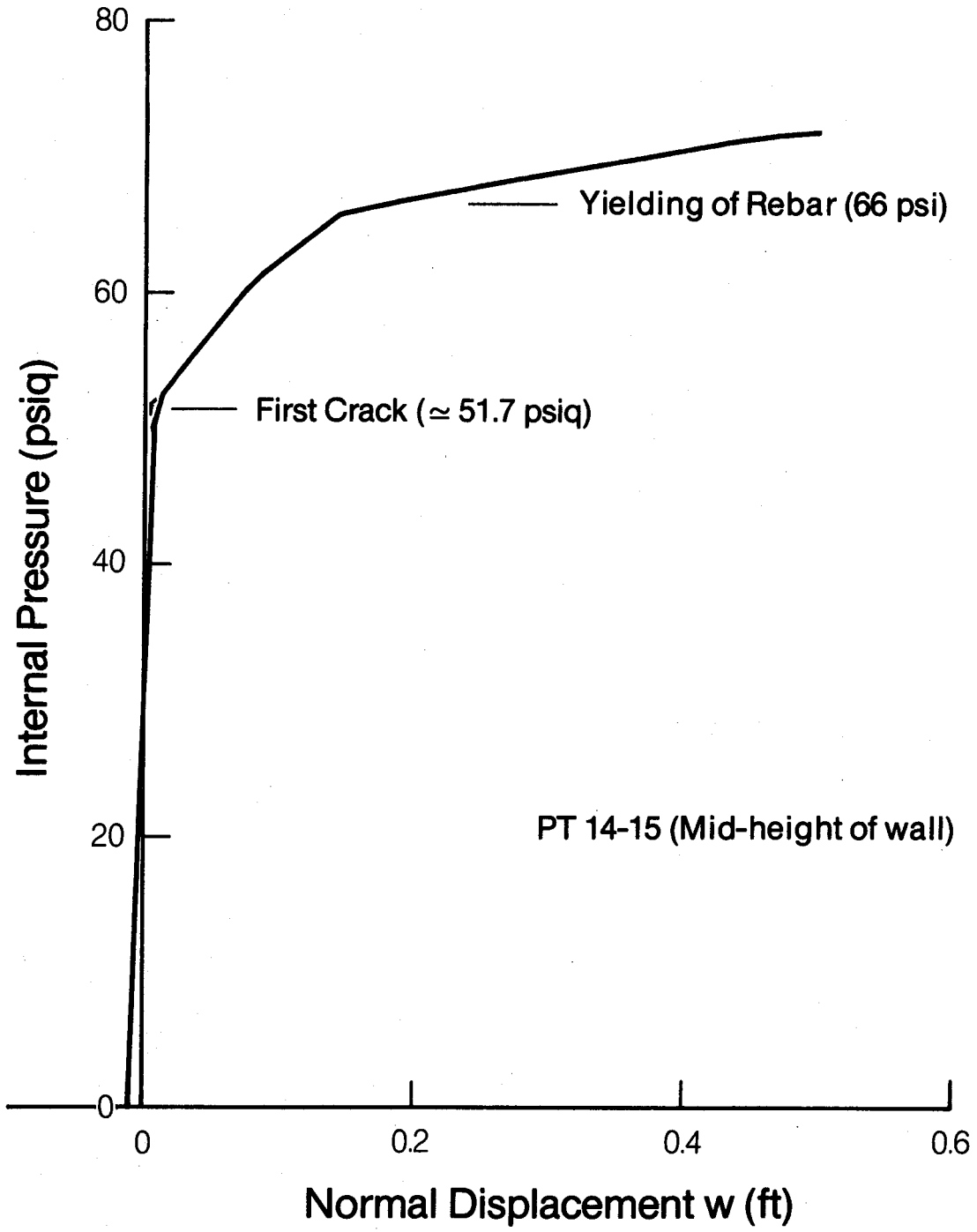

Fig. 3.16 Pressure-Displacement at Mid-height of Wall

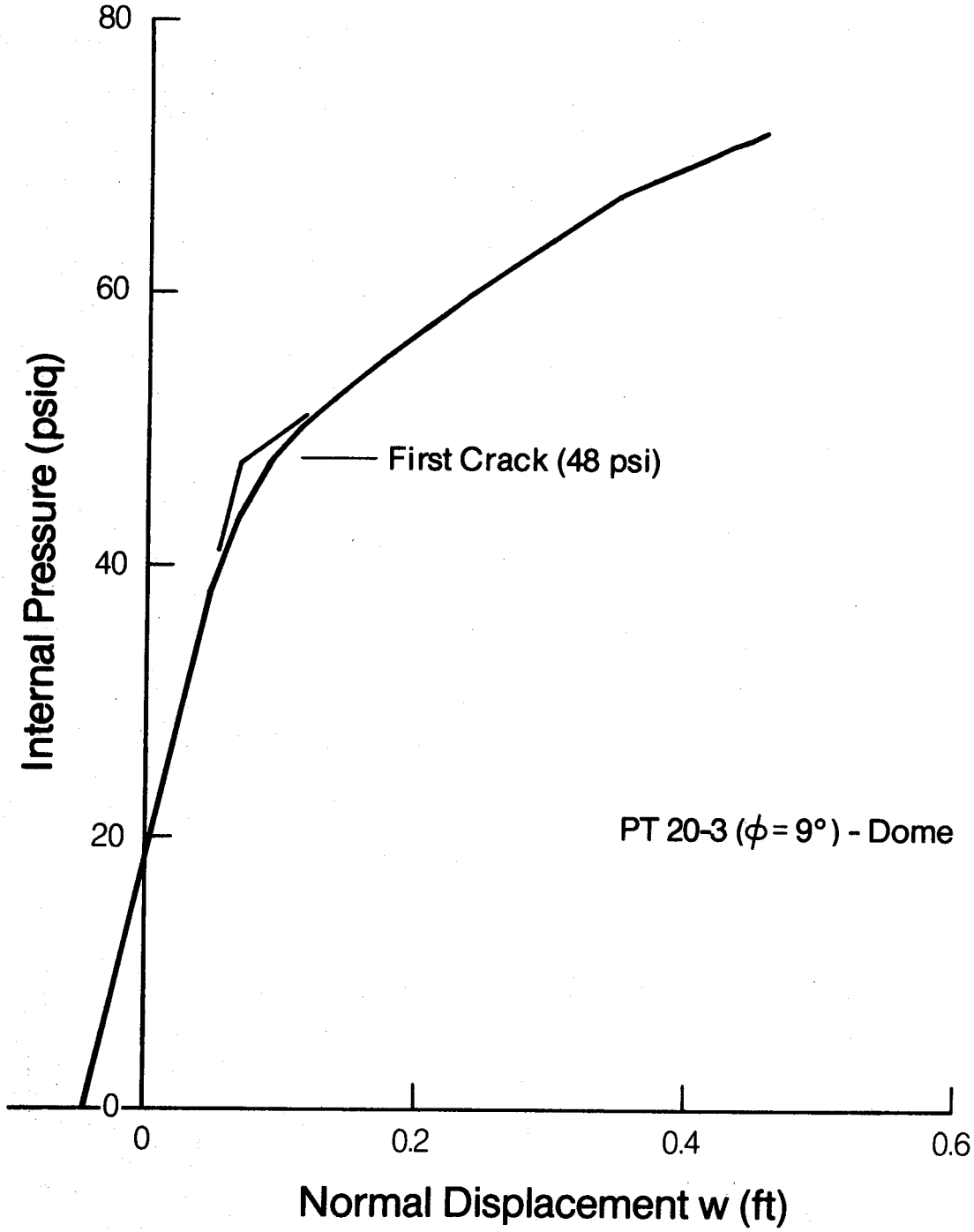

Fig. 3.17 Pressure-Displacement at Crown of Dome

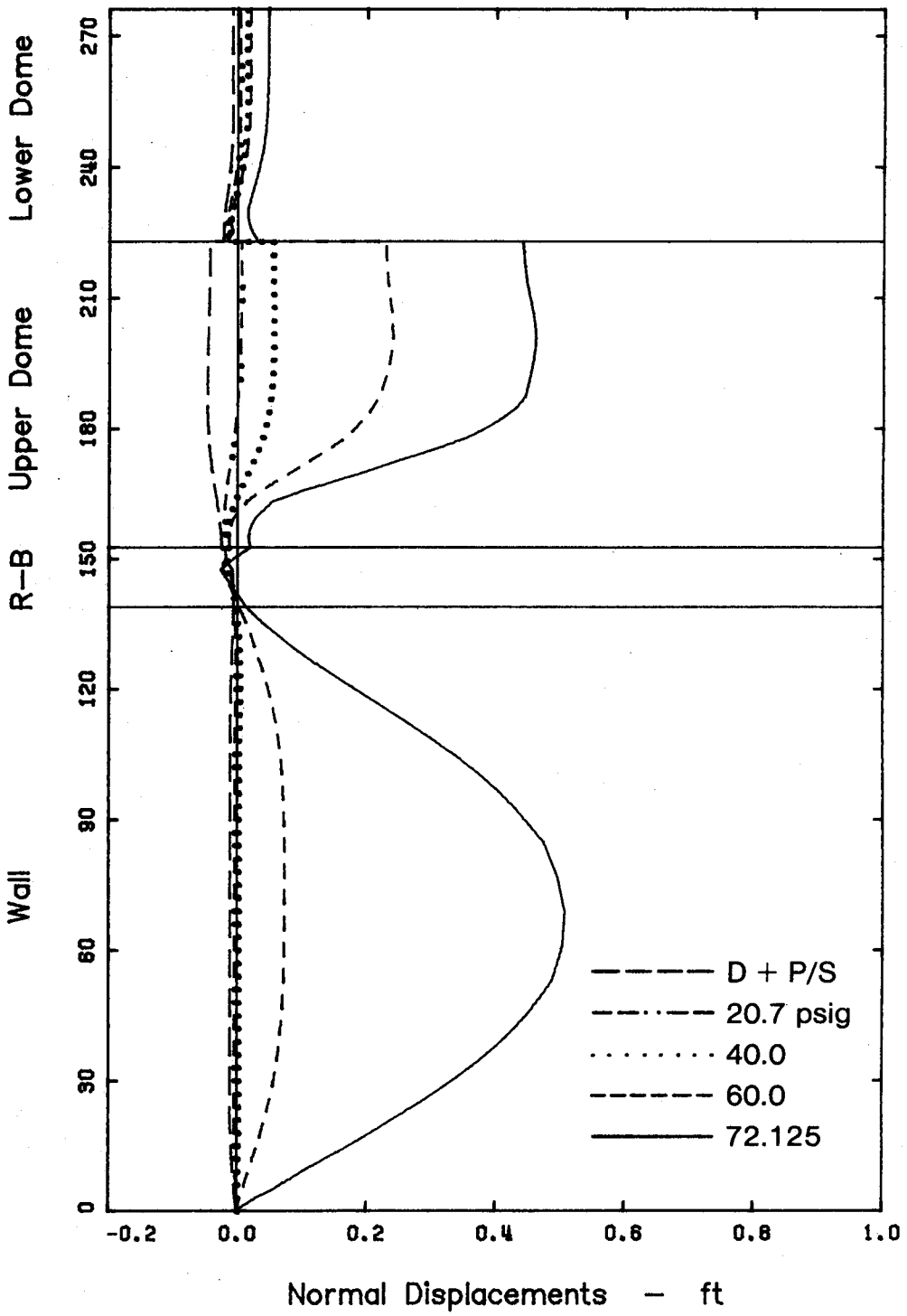

Fig. 3.18 Normal Displacements

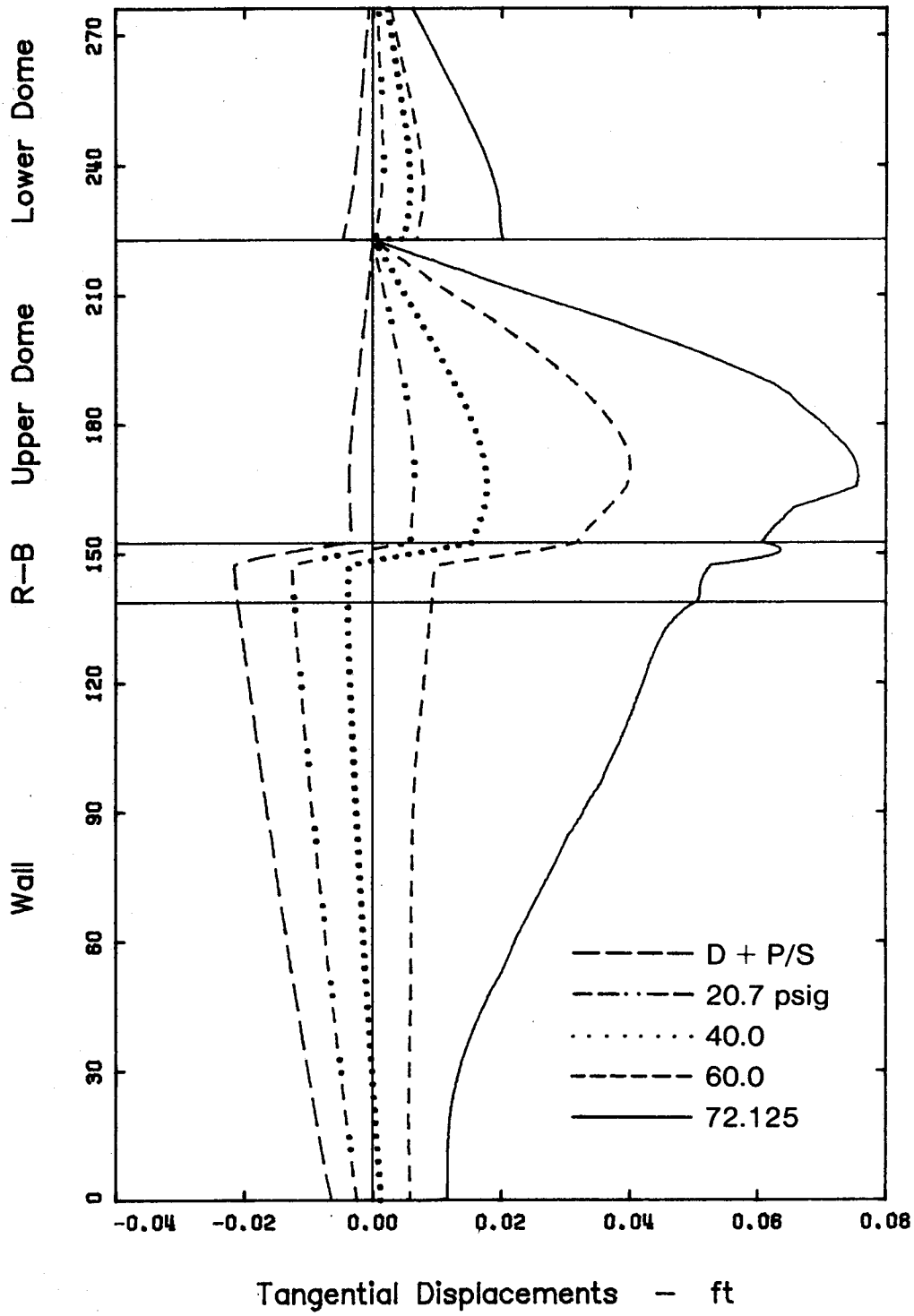

Fig. 3.19 Tangential Displacements

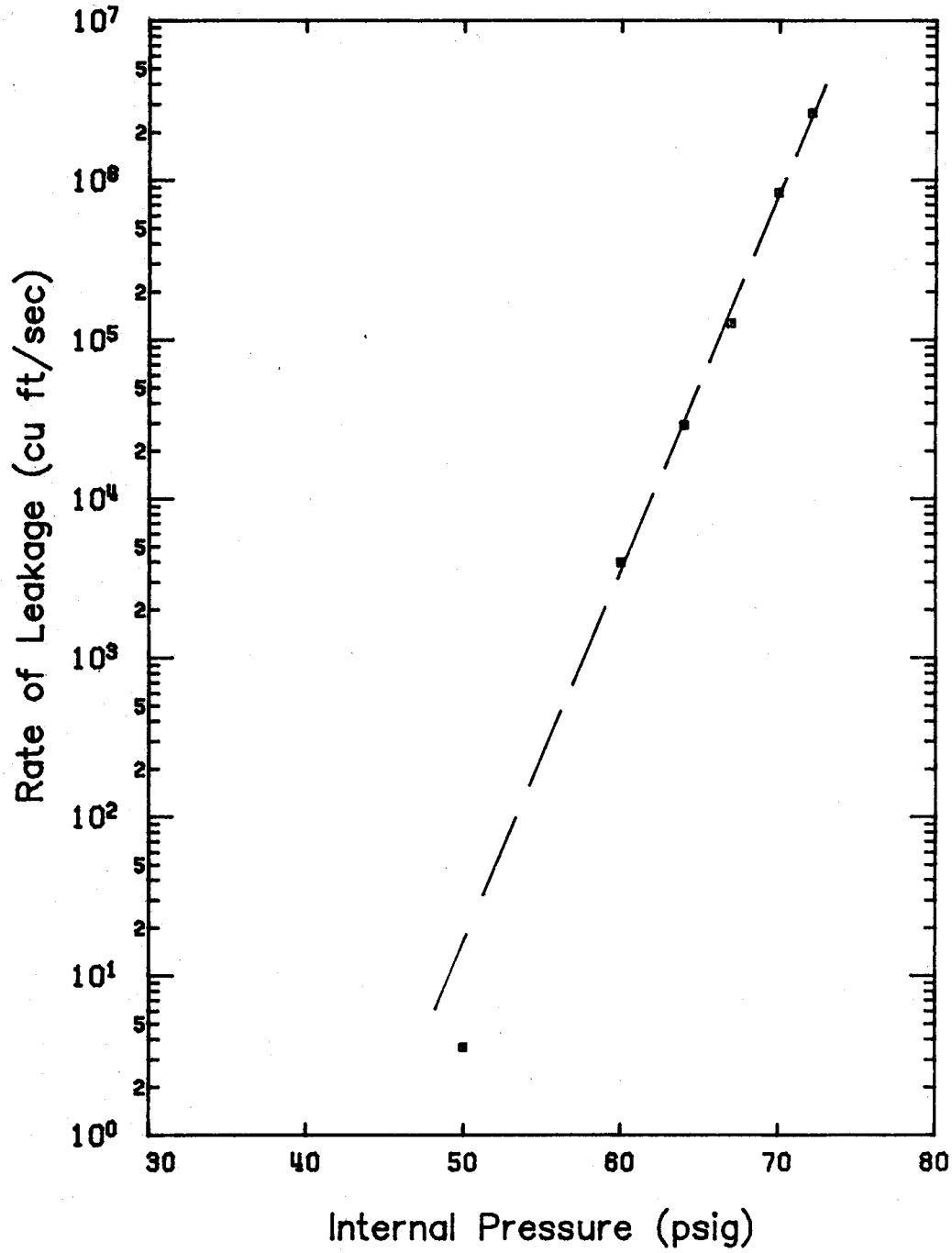

Fig. 3.20 Estimated Leakage Rate

APPENDIX A

Equivalent Axisymmetric Prestressing Net

A.1 Introduction

Since the analysis is axisymmetric it is necessary to convert the properties of the 'equilateral' prestressing net in the dome to an equivalent set of axisymmetric properties. The general technique follows that developed in Ref. 8 but differs in detail because the prestressing net for the test structure was 'orthogonal' rather than 'equilateral'. It was shown in Ref. 8 that nets with cables placed on great circles do not produce a uniform prestressing effect throughout the dome nor do they produce uniform strength and stiffness throughout the dome, even when a constant force exists in all cables. The following analysis makes the assumption that the forces in the cables are constant and, therefore, it ignores friction losses.

A.2 Geometry of the Net

Fig. A1 assumes an equilateral triangle is formed by the net at the crown, with three systems of cables placed at 120° apart on great circles, and with spacing between cables at the crown of s. Spherical geometry can be used to calculate the spacing (in terms of s) and angles between the cables at the springing line, herein assumed to be at an angle of 29.40 from the crown. The results of these computations are shown in Fig. A1 for angles of 0°, 30° and 60° from one of the sets of cables. The sets of cables no longer form triangles. However two sets

form a diamond while the third set is perpendicular to the diagonal of this diamond. The limiting geometries are at 30° and at 0° or 60°.

A.3 Effective Normal Pressure at Crown

Since all cables are assumed to have a constant force of F and spacing s at the crown one may estimate the force per unit of length in the concrete dome by summing force components in the direction parallel to one of the cable systems in the dome and dividing by the distance between the cables.

For the shaded diamond at the crown in Fig. A1 we have, in the 30° direction, a force per unit of length, N_o, of

$$N_o = (2 \cdot F \cdot \frac{1}{2} + 2F)/2s = \frac{3F}{2s} \qquad A.1$$

The normal pressure which would produce this force N is obtained from the simple strength of materials equation

$$p_o = \frac{2N_o}{R} \qquad A.2$$

which, upon substituting A.1, yields

$$p_o = \frac{3F}{Rs} \qquad A.3$$

One may check this simply by recognizing that the normal force per unit length of cable, produced by one cable is the force, F, times the angle subtended by a unit length, $\frac{1}{R}$. Dividing by the cable spacing, s,

yields a normal pressure, and multiplying by three because there are three nets yields Eq. A.3. Thus we have the same result by two techniques. Since the prestressing effect in the dome is produced in the BOSOR5 analysis by applying a normal pressure p, Eq. A.3 serves to determine what this pressure should be at the crown.

Using a force F of 712 kips/cable, a spacing s_o of 3 ft. and a radius of 137 ft., Eq. A.3 yields a normal pressure of 5.197 psf.

The variation of the normal pressure over the dome may now be computed in terms of the crown pressure p_o.

A.4 Variation in Normal Pressure

Accepting the geometry of Fig. A1 we argue that the pressure produced by each set of cables is inversely proportional to the spacing between them. Thus, at 60°,

$$p_{60} = \frac{p_o}{3}\left(\frac{25}{0.90513s} + 1\right) \qquad A.4$$

$$= 1.0699\ p_o$$

Similarly, at 30°,

$$p_{30} = \frac{p_o}{3}\left(\frac{2s}{0.9694s} + \frac{s}{0.8712s}\right) \qquad A.5$$

$$= 1.0703$$

Thus a normal pressure varying from 1.07 p_o at the springing line to p_o at the crown simulates the prestressing effect.

A.5 Variation in Stiffness and Strength Properties

We assume the effective area per unit of width is proportional to the effective force/unit width as computed by resolution of forces. Thus the steel area, A, is assumed proportional to N if the force in the cable is F. This force has been computed at the crown, in the 30° direction, in, Eq. A.1. Similarly at the crown in the 120° direction we have

$$N_o = (2 \cdot F \cdot \frac{\sqrt{3}}{2}) / (\frac{2s}{\sqrt{3}}) = 3F/2s \qquad A.6$$

which checks with Eq. A.1.

Using the subscript ϕ to indicate the meridional direction, and the subscript θ to indicate the circumventional direction we have, from Fig. A1:

(a) At $\theta = 60°$

$$N_\theta = \frac{F \sin 33°.532}{0.98283s \cos 33".532} + \frac{F}{s}$$

$$= 1.67427 \frac{F}{s} = 1.1162 N_o \qquad A.7$$

and

$$N_\phi = \frac{F \cos 33°.532}{0.98283s \sin 33°.532}$$

$$= 1.53537 \frac{F}{s} = 1.0236 N_o \qquad (A.9)$$

and

(b) at $\theta = 30°$

$$N_\theta = \frac{F \sin 63°.298}{1.2074s \cos 63°.298}$$

$$= 1.6466 \frac{F}{s} = 1.0977 N_o \qquad \text{A.9}$$

and

$$N_\phi = \frac{F \cos 63°.298}{1.2074s \sin 63°.298} + \frac{F}{0.8712s} \qquad \text{A.10}$$

Since the area of the prestressing cable is 5.08 in^2, we use Eq. A.1 to find the effective area of prestressing steel per unit width at the crown of the dome as

$$A_o = 3 \times 5.08/2 \times 3$$

$$= 2.54 \text{ in}^2/\text{ft.}$$

At the springing line the critical ratio is given by A.9 in the θ direction and A.8 in the ϕ direction. Hence, we assume that the prestressing net has equivalent circumferential and meridional areas of

$$A_\theta = 1.098 A_o \qquad \text{A.11}$$

$$A_\phi = 1.024 A_o \qquad \text{A.12}$$

at the springing line.

A comparison of the values in this Appendix with those in Ref. 8 indicates that, as expected, an equilateral net gives a more uniform result than an orthogonal net.

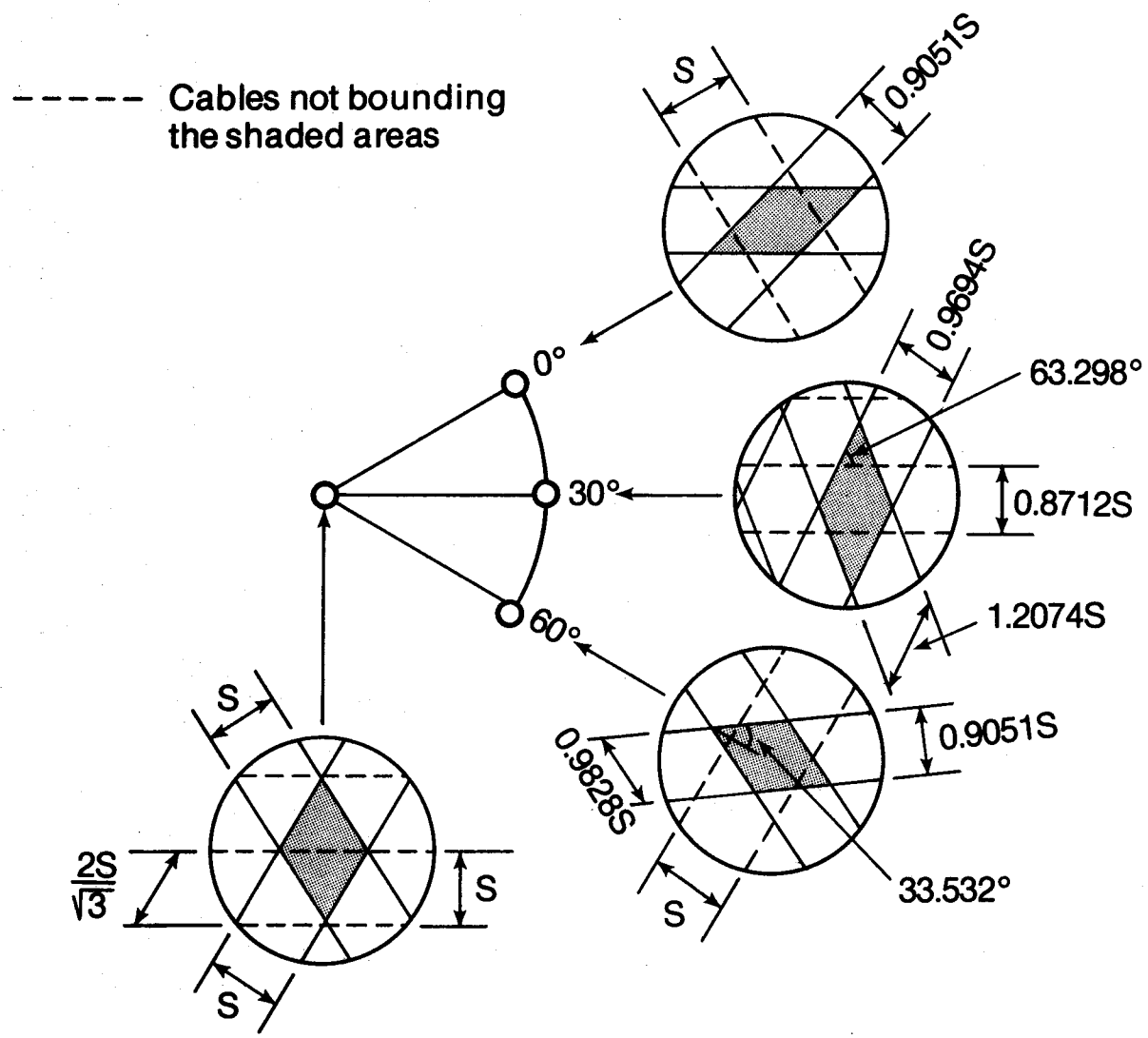

Fig. A1 Equivalent Prestressing Net

APPENDIX B

Ultimate Strength by Membrane Theory

Since the ultimate strength of a containment structure cannot be greater than the ultimate strength of its principal components, and the strength of these components cannot be greater than their tensile membrane capacity, it is a simple matter to compute bounds on the ultimate strength of the structure. The ultimate tensile membrane capacity of the components is simply the capacity of the prestressing and reinforcing steel in the component.

These simple computations are shown in Table B1. It is apparent that the cylinder wall controls the bound on the ultimate strength and this bound is 77.2 psi.

Table B1 - Component Ultimate Strengths

Structural Component	Direction	A_s in^2/ft	A_f in^2/ft	T_u kips/ft.	p_u psig	Formula
Cylinder	θ	1.87	2.53	756	77.2	a
Cylinder	ϕ	1.58	1.30	426	89.3	b
Hinge	ϕ	2.00	1.30	452	94.7	b
Dome	ϕ	2.85	2.54	819	84.3	c

FORMULAE

a: $p = \frac{T_u}{68}$

b: $p = \frac{2T_u}{68^2} \times 69.75$

c: $p = \frac{2T_u}{136^2} \times 13.7$

d: $T_u = A_s f_y + A_f f_{py}$